ACS Infectious Diseases

pubs.acs.org/journal/aidcbc

Article

Identification of 2-Aryl-Quinolone Inhibitors of Cytochrome *bd* and Chemical Validation of Combination Strategies for Respiratory Inhibitors against *Mycobacterium tuberculosis*

Laura N. Jeffreys, Alison Ardrey, Taghreed A. Hafiz, Lauri-Anne Dyer, Ashley J. Warman, Nada Mosallam, Gemma L. Nixon, Nicholas E. Fisher, W. David Hong, Suet C. Leung, Ghaith Aljayyoussi, Jaclyn Bibby, Deepak V. Almeida, Paul J. Converse, Nader Fotouhi, Neil G. Berry, Eric L. Nuermberger, Anna M. Upton, Paul M. O'Neill, Stephen A. Ward, and Giancarlo A. Biagini*

Cite This: https://doi.org/10.1021/acsinfecdis.2c00283

Read Online

ACCESS | Metrics & More | Article Recommendations | Supporting Information

ABSTRACT: *Mycobacterium tuberculosis* cytochrome *bd* quinol oxidase (cyt *bd*), the alternative terminal oxidase of the respiratory chain, has been identified as playing a key role during chronic infection and presents a putative target for the development of novel antitubercular agents. Here, we report confirmation of successful heterologous expression of *M. tuberculosis* cytochrome *bd*. The heterologous *M. tuberculosis* cytochrome *bd* expression system was used to identify a chemical series of inhibitors based on the 2-aryl-quinolone pharmacophore. Cytochrome *bd* inhibitors displayed modest efficacy in *M. tuberculosis* growth suppression assays together with a bacteriostatic phenotype in time-kill curve assays. Significantly, however, inhibitor combinations containing our front-runner cyt *bd* inhibitor CK-2-63 with either cyt *bcc-aa*$_3$ inhibitors (e.g., Q203) and/or adenosine triphosphate (ATP) synthase inhibitors (e.g., bedaquiline) displayed enhanced efficacy with respect to the reduction of mycobacterium oxygen consumption, growth suppression, and *in vitro* sterilization kinetics. *In vivo* combinations of Q203 and CK-2-63 resulted in a modest lowering of lung burden compared to treatment with Q203 alone. The reduced efficacy in the *in vivo* experiments compared to *in vitro* experiments was shown to be a result of high plasma protein binding and a low unbound drug exposure at the target site. While further development is required to improve the tractability of cyt *bd* inhibitors for clinical evaluation, these data support the approach of using small-molecule inhibitors to target multiple components of the branched respiratory chain of *M. tuberculosis* as a combination strategy to improve therapeutic and pharmacokinetic/pharmacodynamic (PK/PD) indices related to efficacy.

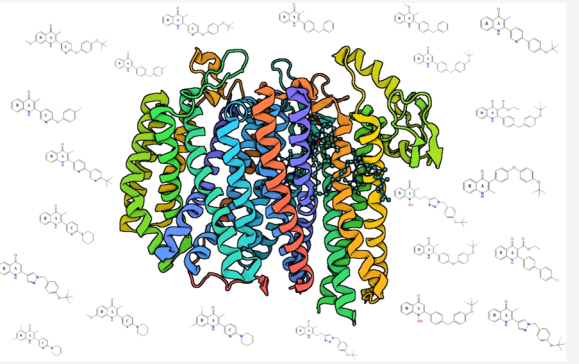

KEYWORDS: *tuberculosis, cytochrome bd oxidase, bedaquiline, Q203*

During the COVID-19 pandemic, the number of deaths caused by tuberculosis (TB) increased for the first time in 10 years, hampering efforts to achieve the WHO TB aims by 2050.[1] While TB prevalence and associated mortality are generally declining, increases in cases of multidrug-resistant (MDR) and extensively drug-resistant (XDR) TB threaten to undermine progress toward reducing the global burden of this disease.[2] The waning efficacy of current therapeutic agents necessitates the development of new drugs, acting against unique targets, which circumvent current resistance mechanisms. Targeting key components of the respiratory chain of *Mycobacterium tuberculosis* have been shown to be effective in sterilizing both replicating and dormant *M. tuberculosis*. Bedaquiline (TMC207, BDQ), the first new TB drug in 50 years and the first drug to specifically target the electron transport chain (ETC) of *M. tuberculosis*, was hoped to combat increasing resistance to front-line drugs such as isoniazid (INH) and rifampicin (RIF).[3−9] This racemic diarylquinoline compound was approved by the FDA for use against multidrug-resistant pulmonary tuberculosis in 2012; however, clinical resistance was reported by 2015.[10] Since then, many other inhibitors of the electron transport chain (ETC) have been discovered: these include squaramides targeting the adenosine triphosphate (ATP) synthase,[11,12] phenothiazines and quinolinyl pyrimidines targeting ndh/ndhA,[9] and various inhibitors targeting cytochrome *bcc* such as imidazopyridines

Received: May 31, 2022

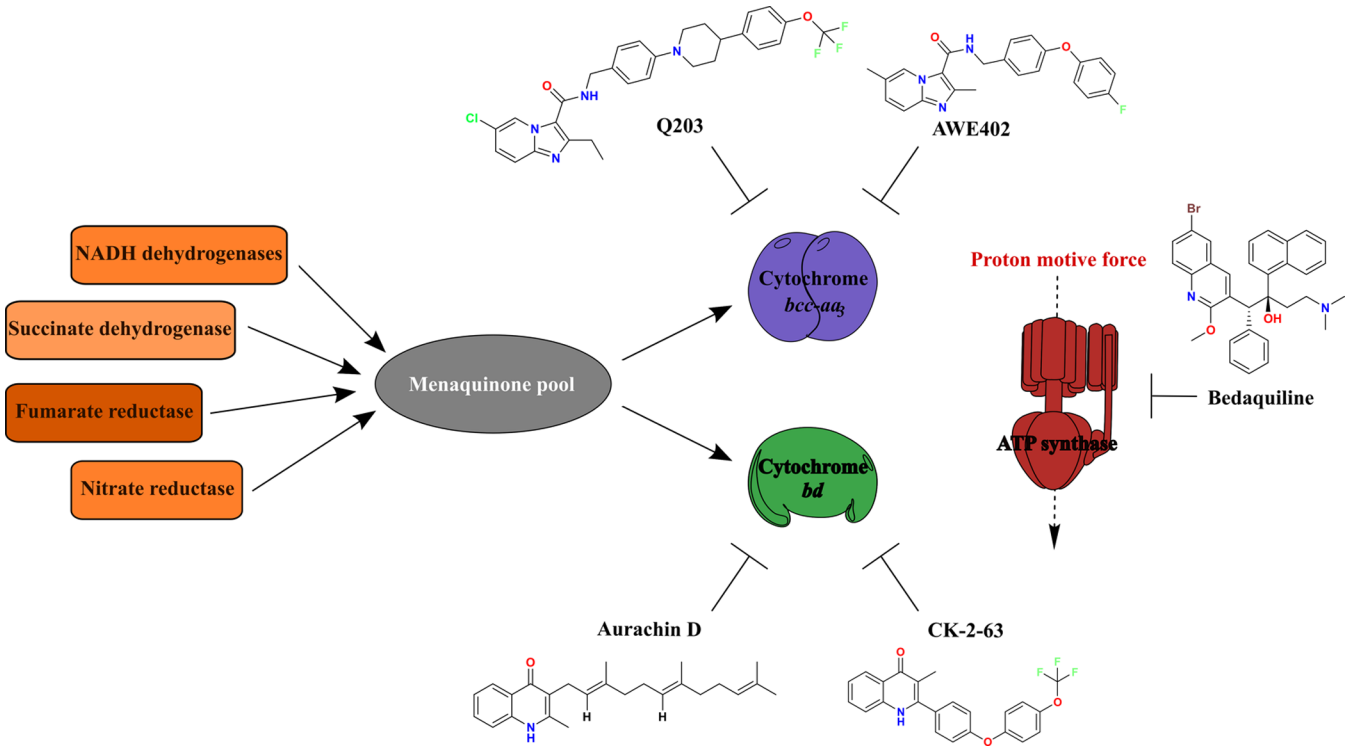

Figure 1. Simplified schematic of the inhibitors of the electron transport chain of *M. tuberculosis*. Electrons (black arrows) are shuttled through the electron transport chain by the reduction and oxidation of menaquinone molecules until the terminal oxygen acceptor is reached. There are several proteins that can be inhibited before this by compounds such as succinate dehydrogenases [e.g., miconazole,[17] triclosan,[18] and 3-nitropropionate[19]] and NADH dehydrogenases [clofazimine[20]]. The terminal oxygen acceptor of the aerobic chain is the cytochrome *bcc-aa*$_3$ supercomplex that can be inhibited by compounds such as AWE402[13] (referred to as compound **17** in Moraski et al., 2013 and named in the patent WO2017103615A1), Q203,[21] and lansoprazole.[15] The terminal oxygen acceptor of the anaerobic chain is cytochrome *bd* oxidase and can be inhibited by the compound aurachin D. During the electron transport chain, several enzymes facilitate the transport of protons from the cytoplasm to the periplasm, generating the proton motive force (dashed arrow) required for ATP synthase to generate ATP, inhibited by compounds such as bedaquiline,[22] squaramides,[11,12] and TBAJ-587.[23,24] The structures of these chemicals are shown in Figure S5.

[e.g., AWE402[13]], 4-(1*H*)-quinolones [e.g., SCR0911[14]], and 2-pyridinylmethylsulfinylbenzimidazoles [e.g., lansoprazole[15]]. One of the more advanced candidates is Q203 (telacebec), targeting the cytochrome *bcc* complex of the ETC, as shown in Figure 1. In Phase 2 clinical studies, increasing doses of telacebec have been reported to be associated with greater reductions in viable mycobacterial sputum load.[16]

The ETC of *M. tuberculosis* has multiple branches that introduce functional redundancy and thereby allow the bacteria to evade inhibition of individual components. Figure 1 is a simplified schematic of two branches of the ETC, both terminating in the consumption of oxygen, and current chemotherapies on the market or in clinical trials. The terminal oxidase cytochrome *bd* quinol oxidase (cyt *bd*) is a putative target from the anaerobic chain. Initially, cyt *bd* was identified as essential for viability in deep sequencing studies;[25] however, in recent studies, deletion of cyt *bd* did not prevent *in vitro* growth[26,27] but did hypersensitize *Mycobacterium* to respiratory inhibitors of cyt bcc[26,28,29] and F_1F_o-ATP synthase.[27] The cyt *bd* complex is expressed predominantly under microaerobic growth conditions and is characterized by its unusually high affinity for oxygen (*Escherichia coli* $K_m[O_2]$ = 5 nM).[30] Present in many prokaryotes including *M. tuberculosis*,[31] *Salmonella typhimurium*,[32] *Klebsiella pneumoniae*,[33] and *Listeria monocytogenes*,[34] cyt *bd* catalyzes the four-electron reduction of molecular O_2 to water. This activity results in the addition to the transmembrane electrochemical gradient that may be harnessed by the cell for a variety of other purposes, most importantly driving ATP synthase.[35,36] Although catalyzing similar chemistry, cyt *bd* exhibits no sequence or structural homology to the widely distributed heme-copper oxidase (HCO) family and is absent in eukaryotes providing an attractive target for treatment.[37−39] Cytochrome *bd* is believed to play a significant role in *M. tuberculosis* adaptation to hostile conditions, with observations that cyt *bd* upregulation has an important role during the transition from acute to chronic disease *in vivo*, exposure to nitric oxide (NO), and hypoxia.[40,41] Furthermore, cytochrome *bd* oxidase upregulation can effectively substitute for impaired cytochrome *bcc-aa*$_3$ supercomplex function during chronic infection, supporting a role for this alternative oxidase in slow growing and/or nonreplicating *M. tuberculosis*.[42,43]

M. tuberculosis cytochrome *bd* oxidase is a membrane-integrated complex encoded by *cyd*A and *cyd*B of the *cyd*ABDC operon.[38,44] *cydDC* encodes a glutathione transporter, demonstrating sequence homology with ATP-binding ABC transporter proteins thought to be essential for cytochrome *bd* oxidase activity.[45,46] Previously, several structures of cyt *bd* have been elucidated from *Geobacillus thermodenitrificans*[47] and *E. coli*.[48,49] Recently, the structure of *M. tuberculosis* cyt *bd* has been reported, which showed greater changes to the Q-loop than predicted from the sequence analysis.[50] Although belonging to the short Q-loop family (e.g., *G. thermodenitrificans*), the PDB structure 7NKZ suggests a Q-loop structure

https://doi.org/10.1021/acsinfecdis.2c00283
ACS Infect. Dis. XXXX, XXX, XXX−XXX

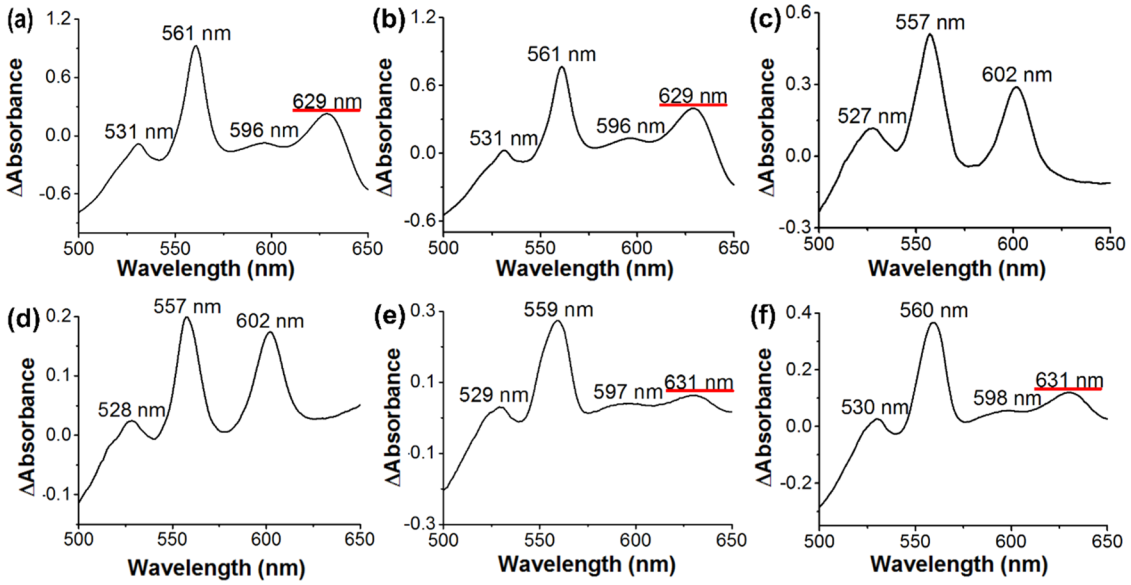

Figure 2. Transformation of *E. coli* cells with the pTMA plasmid encoding cyt *bd* results in restoration of the heme *d* peak. Difference spectra (reduced minus oxidized) of wild-type *E. coli* BL21 (DE3) LysS strain recorded after growth in aerobic (a) and (b) O_2-limited conditions, ML16 double knockout strain in aerobic (c) and (d) O_2-limited conditions, and the transformed TML16 strain, recorded after growth in (e) aerobic and (f) O_2-limited conditions. Wavelengths corresponding to a heme *d* peak are underlined in red, showing successful cyt *bd* overexpression. Measurements were taken at room temperature using sodium dithionite as the reductant and potassium hexacyanoferrate(III) as the oxidant.

closer to the long Q-loop family (e.g., *E. coli*). The catalysis of this complex relies on shuttling electrons between the three heme prosthetic groups, all found within the CydA subunit, in a catalytic cycle mechanism that prevents the formation of reactive O_2 species.[36,47−49,51,52] The role of CydB in the enzyme's catalysis is unclear. However, in *Staphylococci* species, the CydB subunit has been shown to protect cells from respiratory inhibitors such as cyanide.[53]

In this study, we report the first heterologous expression of functionally active *M. tuberculosis* cyt *bd* and describe initial steady-state kinetics of this important enzyme. Further, we identify and characterize the first-in-class cyt *bd* inhibitors (patent WO2017103615A1) and describe their associated *M. tuberculosis* growth inhibitory pharmacodynamics. Significantly, we demonstrate the ability of the lead compound *cyt bd* inhibitor CK-2-63 to potentiate and synergize the growth inhibition and bactericidal activity of known ETC inhibitors including Q203 and BDQ. These data, together with *in vivo* pharmacokinetic (PK) and efficacy data, are discussed in the context of continuing efforts to target the respiratory chain of *M. tuberculosis* toward the development of new antitubercular agents and drug combinations against drug-resistant and persistent *M. tuberculosis*.

RESULTS

Development of a Heterologous *M. tuberculosis* cyt *bd* Expression Platform. The 5.9 kbp *cyd*ABDC operon encoding *M. tuberculosis* cyt *bd* was successfully cloned into the pUC19 expression vector and subsequently transformed to the *E. coli* terminal oxidase knockout strain ML16 (see Methods). Untransformed ML16 harvested cells were yellow/cream. Transforming these cells with cyt *bd* (TML16) resulted in red/brown harvested cells (Figure S1A), indicating overexpression of heme-containing protein(s). SDS-PAGE electrophoresis shows the presence of proteins corresponding to the size of the CydA and CydB domains within transformed cells. These bands are absent or fainter in untransformed cells (Figure S1B).

All the purified cytochrome *bd* enzyme used in subsequent assays was purified from TML16 cells. Following optimization of protein expression, it was determined that the maximal substrate turnover was observed at pH 7.5, while the presence of detergents during purification did not significantly improve the catalytic activity of the membrane preparations (Figure S2).

The difference spectra of wild-type *E. coli* (BL21 (DE3) pLysS) identifies distinctive peaks at 558, 595, and 627 nm, which correspond to the presence of cytochromes b_{558}, b_{595}, and d_{627} of cytochrome *bd* in cells grown aerobically (Figure 2A) or in O_2-limited (Figure 2B) conditions. In the difference spectra of the cytochrome *bo*3/*bd*-I knockout strain ML16 (Figure 2C,D), the peak at ∼630 nm corresponding to cytochrome *d* is absent, while peaks corresponding to heme *b* peaks from other heme-containing proteins are present. The difference spectra of the mutant strain transformed with the *M. tuberculosisbd* encoding plasmid (TML16) show restoration of heme *d* with a peak observable at ∼630 nm (Figure 2E,F). Significantly, while growth in O_2-limited conditions results in decreased cell density, the *M. tuberculosisbd* yield under these conditions is greater, as demonstrated by doubling of the ratio of cytochrome *d*:cytochrome *b* content for both wild-type and TML16 strains.

Initial steady-state kinetic assays were performed with cytochrome *bd* to determine that a catalytically functional coenzyme had been generated. Spectrophotometrically determined kinetic parameters for cyt *bd* in the presence of the molecules decylubiquinol (dQH_2), ubiquinol-1 (Q_1H_2), or ubiquinol-2 (Q_2H_2) (Table S1) revealed an order of substrate preference being established as $dQH_2 > Q_1H_2 > Q_2H_2$. V_{max} values for the three substrates were similar (5−90 μmol·min^{-1}·mg^{-1}) and data generated for dQH_2 and Q_1H_2 obey simple monophasic kinetics to which a Michaelis−Menten function[54] was applied (Figure 3A,B). However, data for Q_2H_2 exhibits

https://doi.org/10.1021/acsinfecdis.2c00283
ACS Infect. Dis. XXXX, XXX, XXX−XXX

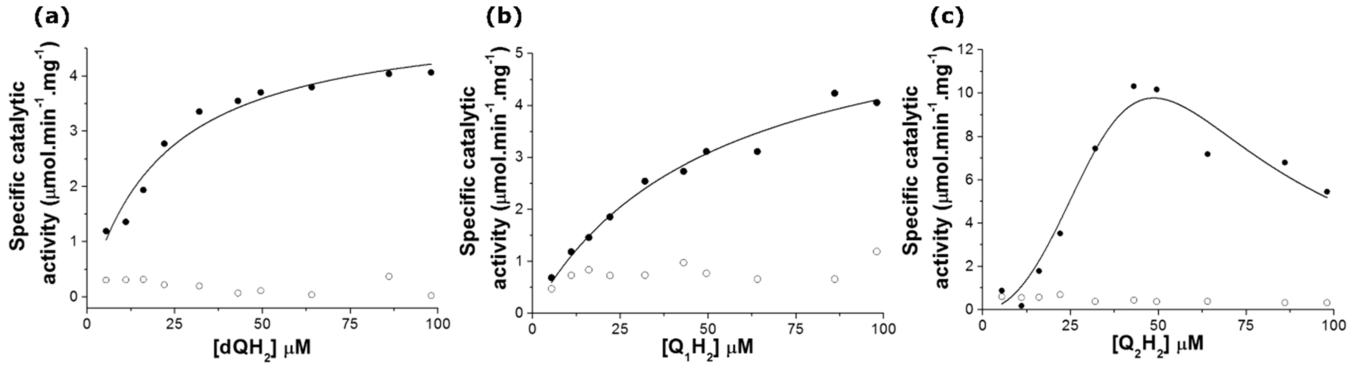

Figure 3. Steady-state kinetics of quinol: *M. tuberculosis* cyt *bd* activity with varying artificial quinol substrates. Steady-state kinetics of *M. tuberculosis* cyt *bd* (TML16) were measured spectrophotometrically at 283 nm (closed circles). ML16 lacking cyt *bd* (open circles) was tested as a negative background. (a) Oxidation of decylubiquinol (dQH_2), apparent K_m (μM), and specific catalytic activity ($\mu mol \cdot min^{-1} \cdot mg^{-1}$) values calculated as 21.52 ± 3.57 and 5.1 ± 0.29, respectively. (b) Oxidation of ubiquinol-1 (Q_1H_2) by *M. tuberculosis* cyt *bd*, apparent K_m (μM), and specific catalytic activity ($\mu mol \cdot min^{-1} \cdot mg^{-1}$) values were calculated to be 51.55 ± 8.9 and 5.26 ± 0.52, respectively. (c) Oxidation of ubiquinol-2 (Q_2H_2) by *M. tuberculosis* cyt *bd*, apparent K_m (μM), and specific catalytic activity ($\mu mol \cdot min^{-1} \cdot mg^{-1}$) values were calculated to be 65.21 ± 15.31 and 8.65 ± 2.5, respectively. Data points are the mean initial rates of experimental duplicates obtained at each quinol concentration indicated. Data for the oxidation of dQH_2 and Q_1H_2 were fitted to a Michaelis–Menten function using rectangular hyperbola, and data for the oxidation of Q_2H_2 were fitted to a modified ping–pong bi–bi function (Origin 8.5 software).

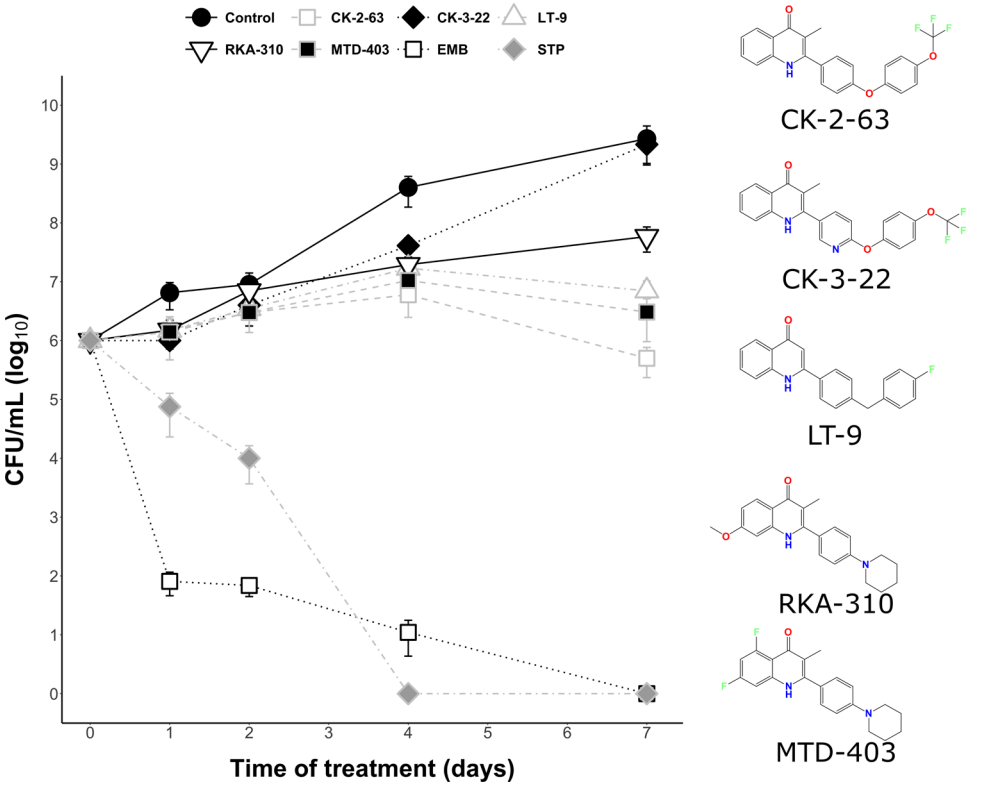

Figure 4. Time-dependent antitubercular activity of selected 2-aryl-quinolone-based cyt *bd* inhibitors in liquid media compared to first-line drugs streptomycin and ethambutol. H37Rv was treated with fixed concentrations ($5xIC_{90}$) of each cyt *bd* inhibitor and two front-line *M. tuberculosis* drugs as positive controls (ethambutol and streptomycin). At each time point, cells were harvested, resuspended in fresh media, and allowed to grow on solid media in the absence of treatment ($n = 3$). All cyt *bd* compounds failed to elicit bacteriocidal effects. Selected compounds are shown here to give representation to each template group.

more complex kinetics: the catalytic activity initially increases as the substrate concentration increases until ~50 μM Q_2H_2 when an inhibitory effect is observed and the cyt *bd* activity decreases significantly. Subsequently, these data required fitting with a modified ping–pong *bi–bi* function to determine K_m and V_{max} values (Table S1 and Figure 3C).

Identification of *M. tuberculosis* Cytochrome *bd* Inhibitors. A focused library of 2-aryl-quinolone compounds from a previous project to target the electron transport chain of *Plasmodium falciparum* was selected for screening against cyt *bd* (Table S2). The compounds demonstrating cyt *bd* activity spanned five quinolone subtemplates (Templates 1–5). Template 1 pyridyl oxygen-linked quinolones[55] demonstrated variable cyt *bd* and *M. tuberculosis* inhibition with CK-3-22 showing the greatest promise for further investigation from this group. Higher ClogP seemed to confer potency within this

https://doi.org/10.1021/acsinfecdis.2c00283
ACS Infect. Dis. XXXX, XXX, XXX–XXX

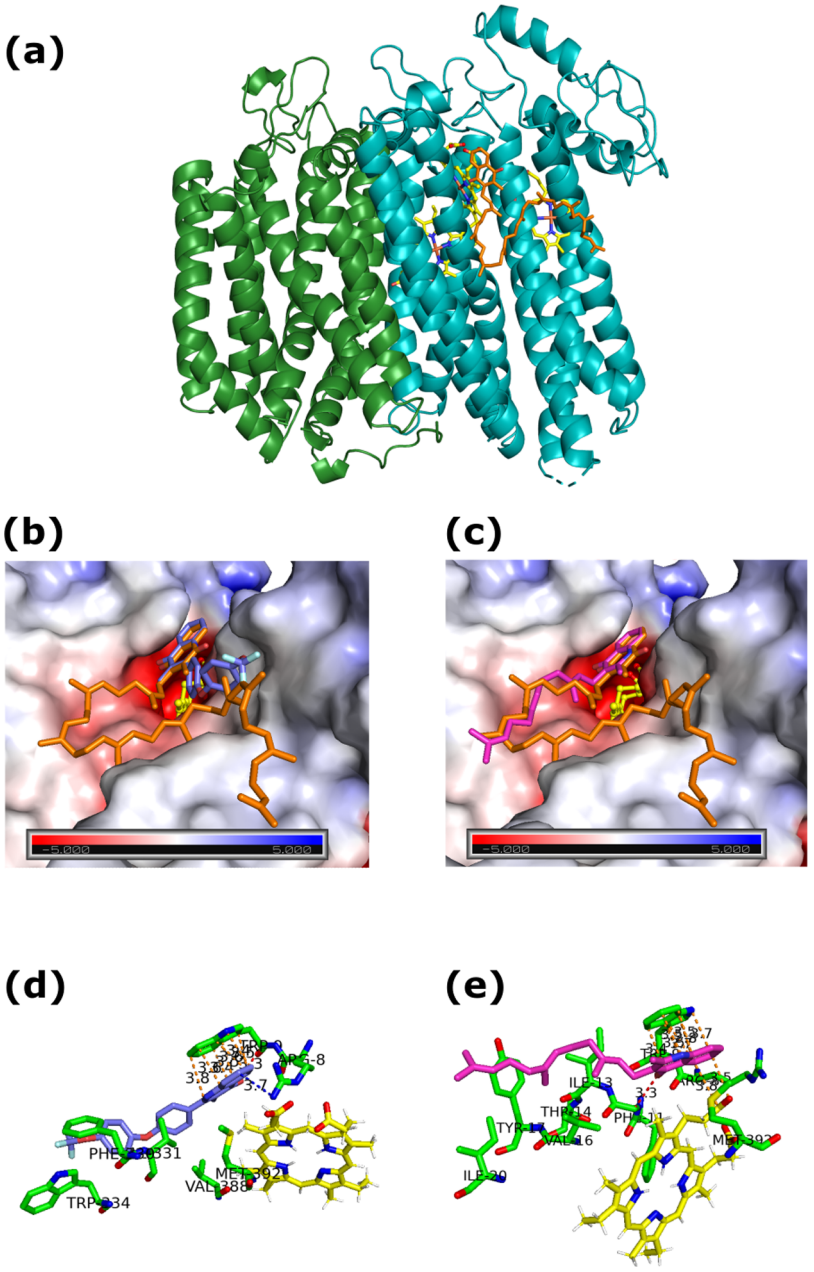

Figure 5. Comparing binding of the lead inhibitor with the known cytochrome *bd* inhibitor aurachin D *in silico*. GOLD 5.2 was used to dock aurachin D or CK-2-63 within the *M. tuberculosis* cyt *bd* structure PDB 7NKZ.[50] (a) CydA domain is shown in blue and the CydB domain is shown in green. The three heme cofactors are shown in yellow sticks. The natural substrate menaquinone was present in this structure during crystallography, shown here in orange sticks. (b) Lead compound CK-2-63 (purple sticks) is overlaid with the natural substrate menaquinone (orange sticks). Using the APBS electrostatics plugin, the charges of the surface amino acids are shown. One of the heme b prosthetic groups in yellow is visible through a solvent-accessible channel. (c) Similar to panel (b), the cyt *bd* inhibitor aurachin D (pink sticks) is shown to interact in the same cleft as menaquinone and CK-2-63. (d) Interactions between CK-2-63 (purple sticks), the amino acids of the CydA domain (green sticks), and the heme prosthetic group (yellow sticks) are shown. $\pi-\pi$ interactions are shown by orange dashed lines, cation−pi bond by blue dashed lines, and hydrogen bonds by red dashed lines. All amino acids labeled interact with CK-2-63 with the dashed lines shown or by Van der Waals interactions (not shown). (e) Similar to panel (d), the interactions between aurachin D (pink sticks), the amino acids of the CydA domain (green sticks), and the heme prosthetic group (yellow sticks) are shown.

template. All Template 2-arylamine quinolones[55] tested were observed to have cyt *bd* activity in the 250 nM to 1.5 μM range with potent antitubercular activity providing a sound basis for further development of the template. Template 3 quinolones[56] containing bisaryl side chains that are either carbon or oxygen-linked provided the most potent cyt *bd* inhibitors, e.g., CK-2-63 (Tables S2 and S3). However, *M. tuberculosis* inhibition while present is not at the same level demonstrated by Template 2, e.g., MTD-403 (Tables S2 and S3). PG-203, an analogue of CK-2-63 with the quinolone side chain at the 3-position as opposed to the 2-position was found to have potent cyt *bd* activity but *M. tuberculosis* growth inhibition was lost (Table S2). Template 4 quinolones[57] have no linker between the aryl groups within the side chain and varying degrees of pyridyl functionality. All compounds within the template demonstrated good cyt *bd* activity but limited *M. tuberculosis*

https://doi.org/10.1021/acsinfecdis.2c00283
ACS Infect. Dis. XXXX, XXX, XXX−XXX

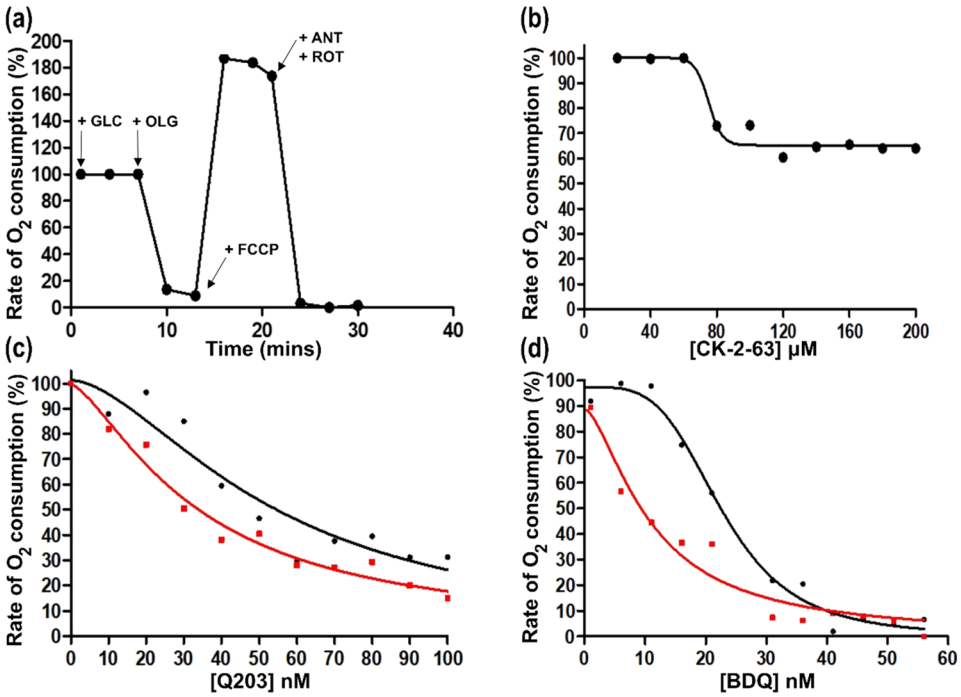

Figure 6. *M. tuberculosis* electron transport chain inhibitors reduce the rate of oxygen consumption in *M. smegmatis*. The rate of oxygen consumption was measured on a Hansatech Oxytherm$^+$ system using high optical density (OD) *M. smegmatis* samples (1 mL; CFU: 7.5×10^6). 10 mM glucose was added, the change in the concentration measured (O_2 nmol mL^{-1}), and used as the 100% oxygen consumption rate before the addition of increasing concentrations of an inhibitor (representative graphs shown here). Panels (b)−(d) were fitted with the Hill function. (a) Arrows represent the time where additions were made: GLC (glucose, 10 mM), OLG (Oligomycin, 15 μM), FCCP (15 μM), ANT (antimycin A, 15 μM), and ROT (rotenone, 15 μM). (b) Lead compound CK-2-63 was able to inhibit oxygen consumption even in aerobic conditions when added in increments over a 60 min period (20−200 μM). (c, d) Sequential addition of Q203 (10−110 nM) or BDQ (1−56 nM) inhibited oxygen consumption in the absence (black) and presence (red) of 3.5 μM CK-2-63.

growth inhibition. Template 5 quinolones[58] have either a pyrazole or triazole present within the side chain. The general trend within this template was modest-poor (μM) cyt *bd* inhibitory activity and limited *M. tuberculosis* growth inhibition.

The steady-state mechanism of cytochrome *bd* inhibition for a selected group of inhibitors (CK-2-63, SL-2-25, MTD-403, PG-203) was further investigated by measuring the inhibition of the enzyme under varying substrate (dQH_2 5−98 μM) and inhibitor concentrations. Data were first fitted to a Michaelis−Menten rectangular hyperbola to calculate K_m and V_{max} (converted to specific catalytic activity) parameters. The data were then transformed to linear Lineweaver−Burk plots (Figure S3). The inhibitory kinetic parameters and the mode of compound inhibition for the four quinolone-based inhibitors are shown in Table S3 and include competitive, uncompetitive, and mixed-inhibition modalities.

Cyt *bd* Inhibitors Suppress Growth Proliferation and Display a Bacteriostatic Phenotype. Compounds displaying inhibition of *M. tuberculosis* cyt *bd* and >50% growth suppression of *M. tuberculosis* H37Rv at 5 μM in a single-point assay were subjected to full IC_{50} determinations under aerobic and O_2-limited (Wayne assay) growth conditions (see Materials and Methods). As detailed in Table S2, all compounds demonstrated *M. tuberculosis* growth suppression, and IC_{50} values under aerobic conditions ranged from 0.27 μM (MTD-403, Template 2) to 3.70 μM (CK-2-63, Template 3). Example dose−response graphs are shown in Figure S4. Under O_2-limiting conditions, all compounds retained their ability to inhibit growth and notably several of these, e.g., CK-2-63 (Template 3) and RKA-310 (Template 2), displayed enhanced potency.

To determine whether growth suppression was due to a bactericidal or bacteriostatic mechanism, time-kill curve studies were performed at $5xIC_{90}$ with a selection of inhibitors (as determined from growth suppression assays). Under the conditions of the assay, untreated *M. tuberculosis* grew at a rate (K_{growth}) of 0.0639 h^{-1}, while the positive controls with known inhibitors streptomycin and ethambutol displayed bactericidal phenotypes with net killing rates (K_{kill}) of 0.17 and 0.44 h^{-1}, respectively (Figure 4 and Table S4). Cyt *bd* inhibitors CK-3-22 (Template 1) showed little to no time-dependent reduction in CFU mL^{-1}, while MTD-403, RKA-310 (Template 2), LT-9 (Template 3), and CK-2-63 (Template 3) displayed net bacteriostatic population phenotypes (Figure 4).

Counter screening of selected compounds against bovine cytochrome *bcc* was performed to identify potential mitochondrial toxicity complications. The data (Table S5) revealed that several compounds have nanomolar activities against bovine cytochrome *bcc*. *In vitro* counter screening of compounds against the immortalized HepG2 cell line showed no appreciable toxicity below 50−100 μM (Table S5). CK-2-63 was chosen as the study's front-runner of the series, given the favorable *in vitro* therapeutic index against the cyt *bd* target.

***M. tuberculosis* cyt *bd* Inhibitors Predicted to Bind in the Menaquinone Binding Pocket.** Using the structure of cytochrome *bd* from the recent cryo-EM structure,[50] the bindings of the inhibitors aurachin D and CK-2-63 were modeled (Figure 5). Aurachin D is a small molecule known to inhibit several proteins of the ETC with some preference for

https://doi.org/10.1021/acsinfecdis.2c00283
ACS Infect. Dis. XXXX, XXX, XXX−XXX

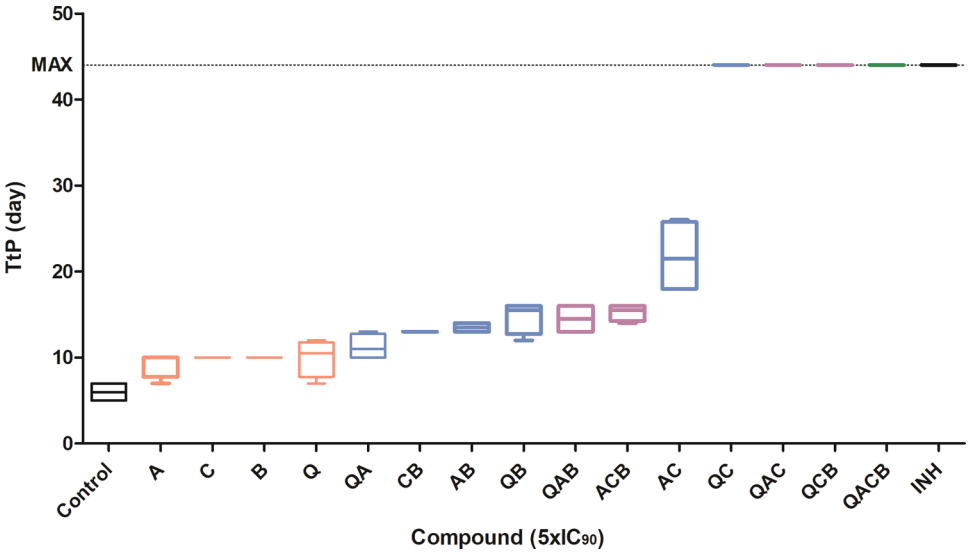

Figure 7. Combination therapy approaches lead to increases in time to positivity (TTP). The time to positivity (TtP) was measured for several ETC inhibitors alone and in combination at equipotent ($5xIC_{90}$) concentrations. Growth suppression of *M. tuberculosis* increases the TtP (>44 days indicates maximum measurable suppression of growth). Inhibitors included Q203 (Q, cytochrome *bcc-aa*$_3$ inhibitor), AWE402 (A, cytochrome *bcc-aa*$_3$ inhibitor), CK-2-63 (C, cytochrome *bd* inhibitor), and bedaquiline (B, ATP synthase inhibitor). All conditions were performed with technical and biological duplicates and ordered by TtP. Controls are shown in black, drugs in isolation in red, dual combinations in blue, triple combinations in purple, and the quadruple combinations in green.

cytochrome *bd*. The ligands were docked using a previously studied genetic algorithm.[59] Docking solutions found were very similar to each other in terms of the location of binding, conformation of ligand, and docking score (PLP score 89.65 ± 2.4).

Both ligands bind in the menaquinone binding pocket located near the Q-loop and one of the heme b prosthetic groups necessary for catalysis. This critical binding site likely suggests these compounds act as noncompetitive or mixed inhibitors for the natural substrate menaquinone. Indeed, kinetics observed with our recombinant enzyme suggested that CK-2-63 exhibited mixed inhibition at 4 nM (Figure S4 and Table S3). Using the APBS electrostatic plugin, the surface charge of the proteins within this binding site were visualized. Although the solvent-accessible channel to the heme *b* prosthetic group is highly negatively charged, the binding site is fairly neutral (Figure 5B,C).[60] Many amino acids were found to interact with aurachin D and CK-2-63 such as Met392, Arg8, and the heme *b* prosthetic group via a propionate group. However, most residues were unique to each inhibitor molecule. Both compounds make $\pi-\pi$ interactions with Trp9 using their aromatic rings at the end of the molecule in closest proximity to the heme prosthetic group. Interestingly, CK-2-63 also makes a cation$-\pi$ interaction with Arg8 (3.7 Å), while aurachin D makes a hydrogen bond with ILE13 (3.3 Å). Both compounds also make numerous Van der Waals interactions across the whole length of the molecules.

Dual Targeting of cyt *bd* and cyt *bcc* or ATP Synthase Results in Enhanced Inhibitory Profiles. We next explored the pharmacodynamic effect of inhibiting multiple components of the ETC with small-molecule inhibitors, including the described cyt *bd* inhibitors, using several different approaches to measure functional cellular bioenergetics, growth, and viability.

The first approach that was investigated assessed the oxygen (O_2) consumption rate (OCR) of *Mycobacterium smegmatis* and the effect of various ETC inhibitors such as antimycin A (ANT) or mycobacteria-specific compounds such as Q203, bedaquiline, and CK-2-63 (Figure 6). The rate of O_2 consumption was calculated by measuring the rate of glucose consumption in the electrode chamber for 2 min prior to the addition of the inhibitor, representing 100% O_2 consumption. As sequential additions of the inhibitor were added, the rate of O_2 consumption decreased. The O_2 consumption of *M. smegmatis* performed as expected with known inhibitors as shown in the Seahorse assay (Figure 6A). Briefly, basal respiration is established using glucose as the carbon source, oligomycin (OLG) inhibits ATP-linked respiration (complex V), FCCP is a protonophore that collapses the inner membrane gradient causing an increase in O_2 consumption to the maximal respiratory rate, and finally the addition of antimycin A (ANT) and rotenone (ROT) inhibit complexes III and I, respectively, inhibiting the ETC fully. CK-2-63 was able to partially inhibit O_2 consumption, though only at very high concentrations (Figure 6B). In contrast, Q203 and BDQ were able to inhibit O_2 consumption at low concentrations, with BDQ eliminating oxygen consumption over the course of the assay (1 h). Significantly, the addition of a fixed concentration (3.5 μM) of CK-2-63 increased the inhibitory effect of Q203 and BDQ across a range of concentrations (Figure 6C,D).

Mycobacterial growth indicator tubes (MGIT) were used to determine the capability of ETC inhibitors, alone or in combination, to suppress the growth of *M. tuberculosis*. MGIT tubes are widely used for the detection and recovery of *M. tuberculosis* from patient samples and measure *M. tuberculosis* growth indirectly via fluorescence measurement of dissolved O_2.[61] Fluorescence measurements can be taken continuously during *M. tuberculosis* growth, and the time taken (days) to reach maximum growth (a reading of over 14 au) is referred to as the time to positivity (TtP). Addition of ETC inhibitors as monotherapies resulted in modest increases in the TtP of *M. tuberculosis* relative to untreated controls, from 10 days for the cyt *bd* inhibitor CK-2-63, to increases of 10−12 days for cyt

https://doi.org/10.1021/acsinfecdis.2c00283
ACS Infect. Dis. XXXX, XXX, XXX−XXX

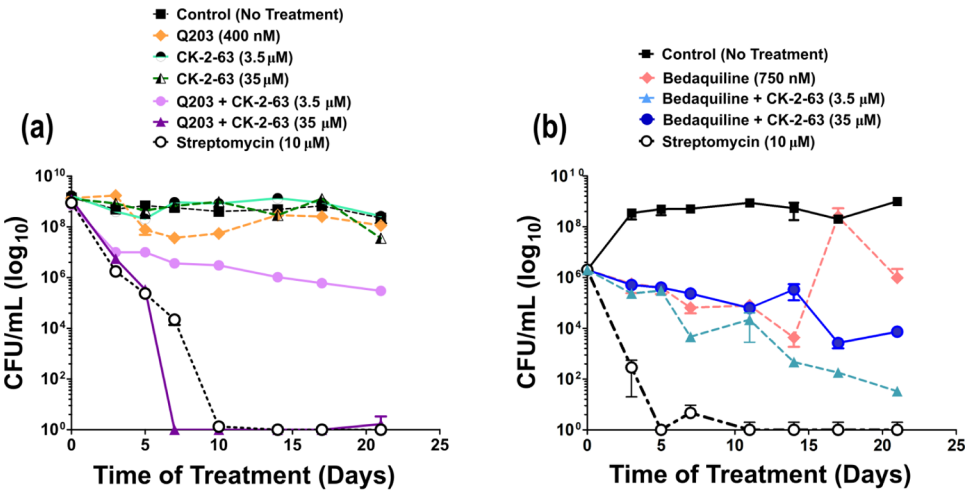

Figure 8. CK-2-63 combination therapies lead to sterilization in time-kill experiments. Similar to Figure 4, H37Rv was treated with BDQ (MIC_{90} = 0.05 μM), Q203 (MIC_{90} = 0.02 μM), and/or CK-2-63 (MIC_{90} = 5 μM) for up to 21 days in liquid culture before addition to solid culture in the absence of inhibitors (n = 3). Suboptimal concentrations of bedaquiline result in regrowth of *M. tuberculosis*. Treatment with bedaquiline or Q203 failed to greatly reduce CFU mL^{-1}. Sterilization by low concentrations of bedaquiline or Q203 is achieved by the addition of the lead cyt *bd* inhibitor CK-2-63.

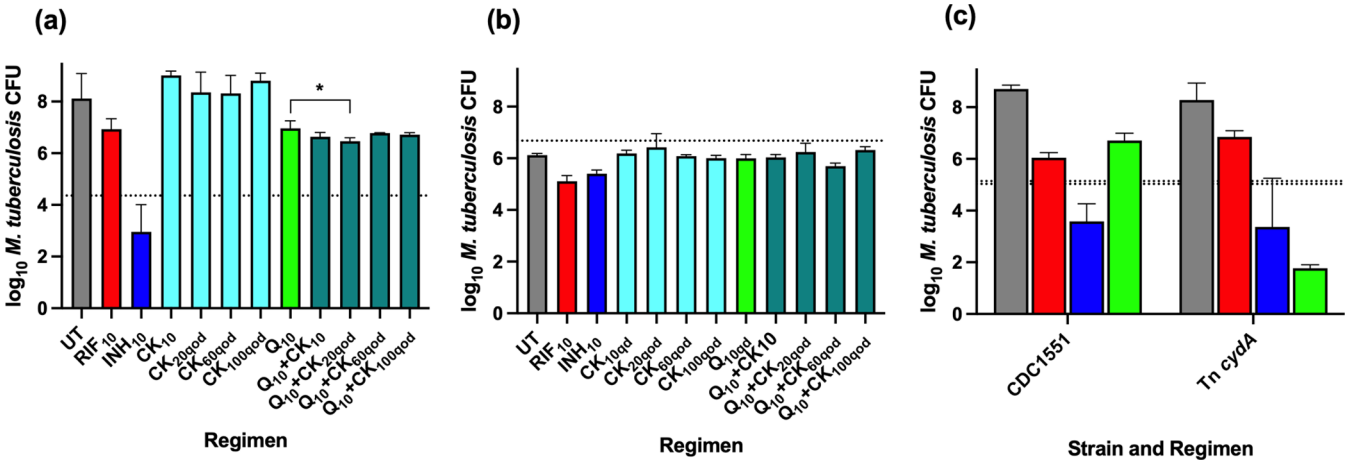

Figure 9. Assessment of combination therapy of ETC inhibitors using acute and chronic in vivo mouse models of TB infection. Mtb H37Rv bacterial burdens were determined from BALB/c mice using (a) acute or (b) chronic infection models. Treatment arms included RIF (red bars), INH (dark blue bars), Q203 (green bars), CK (light blue bars), Q+CK (blue-green bars), and untreated (gray bars) for 1 month. The mean bacterial burden in the untreated mice at the initiation of treatment (day 0) is shown with a dashed line. Numerical values in the regimens indicate doses in mg kg^{-1}. qd indicates once daily dosing Mon−Fri. qod indicates dosing on Mon, Wed, and Fri only. In the acute model (a), all treatments, except for CK monotherapy, showed statistically significant ($p < 0.05$) reductions in bacterial burden compared to the untreated group. $Q+CK_{20}$ (indicated with asterisk) was statistically significantly more active than Q alone (p = 0.0044). In the chronic model (b), statistically significant differences were observed only between untreated mice and mice treated with INH or RIF (p = 0.0004 and $p < 0.0001$, respectively). (c) Mice infected with Mtb CDC1551 (left) or the *cydA* transposon mutant (right) in the acute model were treated with 10 mg kg^{-1} of RIF, INH, or Q203 for 1 month. The mean bacterial burden in the untreated mice at day 0 is shown with dashed lines. Compared to untreated mice, there were significant reductions in bacterial burden after treatment with all three drugs in mice infected with CDC1551 ($p < 0.0001$, $p < 0.0001$, and p = 0.0007). In mice infected with the transposon mutant, there were significant reductions only in mice treated with INH and Q203 (p = 0.0008 and 0.0001, respectively) but not in mice treated with RIF. There was no significant difference in the bacterial burden in untreated mice infected with either strain. However, in mice treated with Q203, the bacterial burden was significantly lower for the *cydA* mutant than the wild-type strain ($p <$ 0.0001). Bars show the mean of data (n = 4) and the error bars show the standard deviation. Group means were compared by one-way ANOVA with Dunnett's post-test correction for multiple comparisons.

bcc-aa$_3$ inhibitors Q203 and AWE402[13] and the complex V inhibitor BDQ (Figure 7). However, combination therapies of CK-2-63 with inhibitors of other ETC components led to large increases in TtP, up to the maximum measurable period of 44 days when combined with Q203. Moreover, multicomponent triple combination therapies, consisting of cyt *bcc*, ATP synthase, and cyt *bd* inhibitors led to maximum measurable increases in TtP, matching the isoniazid positive control. Despite the impressive bacteriocidal qualities of isoniazid in the *in vitro* experiments leading it to become the common positive control in such experiments, single drug treatments in clinical settings lead to resistant strains due to the presence of persister populations.[62]

To determine whether combining ETC inhibitors resulted in enhanced sterilization rates of *M. tuberculosis*, we conducted time-kill studies. Treatment of *M. tuberculosis* with the cyt *bd*

https://doi.org/10.1021/acsinfecdis.2c00283
ACS Infect. Dis. XXXX, XXX, XXX−XXX

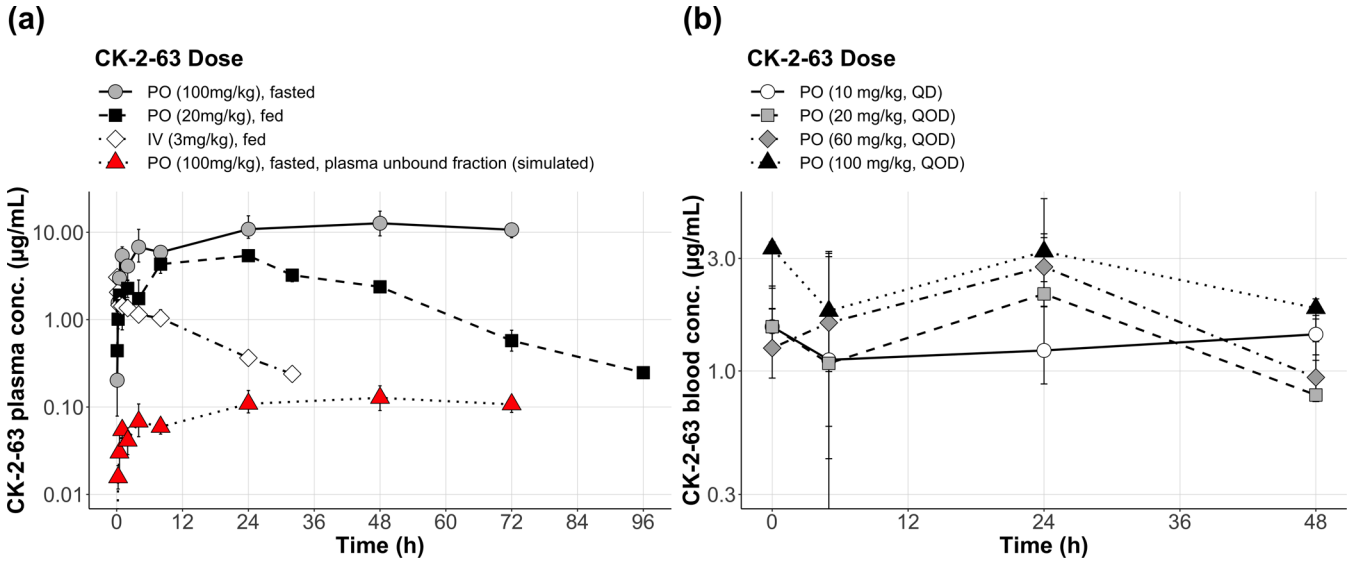

Figure 10. Pharmacokinetics of CK-2-63 in mice. (a) Plasma exposure to CK-2-63 after single dose via oral (100, 20 mg kg^{-1}) or IV (3 mg kg^{-1}) administration. The predicted exposure to the plasma unbound fraction is also shown in red triangles that assumed a best case scenario of 99.7% plasma protein binding. (b) Whole blood exposure at steady state after increasing doses administered orally (10 mg kg^{-1} once daily (QD), or 20, 60, 100 mg kg^{-1} administered every other day (QOD)). Points show the median of data [(a) $n = 2$, (b) $n = 3$] and the error bars show the range of data.

inhibitor CK-2-63 alone, up to 35 μM had little to no sterilizing effect, while treatment with the cyt *bcc-aa*$_3$ inhibitor Q203 (400 nM) resulted in a modest (0.6 log reduction) sterilization (Figure 8A). However, significantly, a combination of CK-2-63 and Q203 resulted in a substantial increase in the sterilization rate of *M. tuberculosis*, exceeding the rate of kill with streptomycin when combined at higher (35 μM) concentrations of CK-2-63. Time-kill curves of BDQ alone or in combination with CK-2-63 were also performed. Similarly, as seen with Q203, when CK-2-63 was combined with BDQ, especially at suboptimal concentrations of BDQ, significant enhancement of *M. tuberculosis* sterilization was observed (Figure 8B).

Determination of *In Vivo* Antitubercular Efficacy Enhancement by Combination Therapies Containing the cyt bd Inhibitor CK-2-63. Two inbred mouse models of TB disease that mimic acute and chronic infection were used for the evaluation of antitubercular efficacy enhancement by combination therapies containing the *cyt bd* inhibitor CK-2-63. The aim of this approach was to assess target vulnerability during specific phases of infection where bacteria are enriched for those either actively replicating (i.e., acute TB) or slow/nonreplicating bacilli (i.e., chronic TB). As expected in the acute TB model, untreated controls succumbed to the infection or required euthanasia during the fourth week post-infection with the *M. tuberculosis* H37Rv strain (second week of the treatment period). Treatment with 10 mg kg^{-1} once daily (QD) exhibited isoniazid (INH) bactericidal activity, reducing the lung *M. tuberculosis* burden below the burden present at the start of the treatment, while 10 mg kg^{-1} of rifampicin (RIF) or Q203 daily allowed a net increase in *M. tuberculosis* burden during the treatment period but not to the extent observed in untreated controls, and each of these treatments prevented death (Figure 9A). However, treatment with CK-2-63 10 mg kg^{-1} administered daily or up to 100 mg kg^{-1} administered thrice weekly (QOD) failed to significantly reduce the growth of *M. tuberculosis* in the lungs and all mice treated with CK-2-63 died or required euthanasia in a time frame similar to untreated mice. Treatment with combinations of Q203 and CK-2-63 resulted in modestly lower lung burden than treatment with Q203 alone, although only the Q203 plus CK-2-63 20 mg kg^{-1} QOD arm was statistically significantly different from Q203 alone ($p = 0.0043$), calculated by one-way analysis of variance (ANOVA) with Dunnett's post-test (Figure 9A). In the chronic TB disease model of infection with *M. tuberculosis* H37Rv, while both RIF and INH treatment resulted in a reduction of *M. tuberculosis* burden in the lungs, treatment with Q203 10 mg kg^{-1} or with CK-2-63 up to 100 mg kg^{-1} (QOD), or Q203 and CK-2-63 in combination, failed to significantly reduce *M. tuberculosis* burden in the lungs (Figure 9B). In a further acute mouse model study using mice infected with either the CDC1551 wild-type *M. tuberculosis* strain or an isogenic *M. tuberculosis* mutant with an inactivating transposon insertion in *cydA*,[63] treatment with INH 10 mg kg^{-1} QD was bactericidal and RIF 10 mg kg^{-1} QD largely bacteriostatic against both the CDC1551 parent strain and the *cydA* transposon insertion mutant. However, treatment with Q203 10 mg kg^{-1} QD resulted in substantial bactericidal activity superior to INH in the lungs of mice infected with the *cydA* mutant but was not even bacteriostatic in mice infected with the wild-type CDC1551 strain, thus confirming the marked susceptibility of *M. tuberculosis* to Q203 in the absence of a functional cyt *bd*.

In vivo murine pharmacokinetic (PK) studies were carried out for CK-2-63 (Figure 10). The PK of CK-2-63 after intravenous (i.v.) and oral (p.o.) administration in mice showed that the concentrations of CK-2-63 decreased rapidly following i.v. administration. C_{max} was reached 24−48 h after p.o. administration of CK-2-63, indicating slow absorption and bile recycling. The area under the plasma concentration−time curves (AUCs) of CK-2-63 increased nonlinearly with the p.o. dose between 20 and 100 mg kg^{-1}, although this observation is confounded by the feeding status (Table S6). Increases in steady-state CK-2-63 exposures were also less than dose-proportional in the whole blood of *M. tuberculosis*-infected mice receiving 20, 60, or 100 mg kg^{-1} QOD. Bioavailability

https://doi.org/10.1021/acsinfecdis.2c00283
ACS Infect. Dis. XXXX, XXX, XXX−XXX

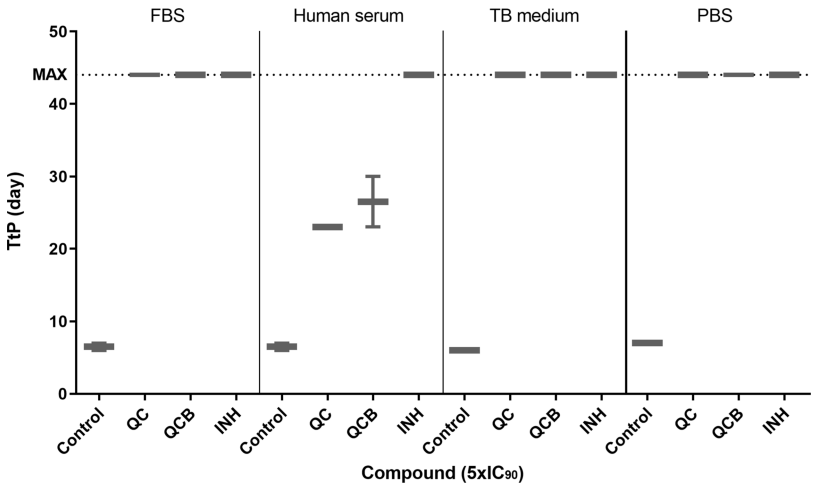

Figure 11. Addition of human serum reduces the efficacy of CK-2-63 in liquid culture. MGIT tubes were supplemented with 10% v/v fetal bovine serum (FBS), human serum, 7H9 (TB) medium, or phosphate buffered saline (PBS) in technical duplicate. Q corresponds to Q203, C corresponds to CK-2-63, B corresponds to bedaquiline, and INH to the positive control isoniazid. The dashed line represents the length of time required in clinical settings to be determined as negative for an active TB infection. The time to positivity observed was decreased for many treatments in the presence of human serum, including for the previously successful Q203 and CK-2-63 combination with or without bedaquiline.

(F) was approximated to be 39.4% (based on 3 mg kg^{-1} IV dose and 20 mg kg^{-1} oral dose). Plasma protein binding of CK-2-63 was determined to be high (>99.9% for 1 μM CK-2-63 and 99.7% for 10 μM CK-2-63) for both mouse and human plasma, as determined using QTrap 4500 MS-based detection system (see Methods). These data indicated that during the *in vivo* murine PK and PK/PD studies, the concentrations of unbound CK-2-63 are significantly lower than the measured total CK-2-63 concentrations (Figure 10).

To further investigate the effect of the high plasma binding of CK-2-63, the MGIT combination experiments detailed above were repeated in the presence of 10% (v/v) human serum and compared with fetal bovine serum (FBS), 7H9 TB media, or phosphate buffered saline (PBS) controls (Figure 11). In the presence of media only (7H9 control), or following addition of FBS or PBS, combination of CK-2-63 and Q203 or the triple combination of CK-2-63, Q203, and BDQ resulted in large increases in TtP, up to the maximum measurable period of 44 days (Figure 11). However, following the addition of 10% (v/v) human serum, all treatments exhibited lower times to positivity, including the previously successful dual and triple combinations (Figure 11). There was no change between the controls lacking drug treatment but with different supplements, including 10% (v/v) human serum.

DISCUSSION

We report the first biophysical characterization of recombinant *M. tuberculosis* cytochrome *bd* quinol oxidase. Restoration of the cytochromes *b* and *d* peaks at 596 and 630 nm by the introduction of the pTMA plasmid confirms successful expression, folding, and incorporation of *b* and *d* type hemes for the encoded protein (Figure 2). The spectrum of our recombinant protein is comparable to other cyt *bd* protein spectra present in the literature, including for the recombinant *M. tuberculosis* cyt *bd* protein recently used to produce cryo-EM structures.[50] Further confirmation of the catalytic activity of *bd* was demonstrated by steady-state kinetic analyses performed using membrane preparations (Table S1). Data, with the exception of Q_2H_2, fit to Michaelis−Menten hyperbola and indicate a preference for dQH_2 as the substrate (Figure 3). K_m values for the three substrates tested are comparable to affinities observed for other well-characterized organisms, e.g., *E. coli*, *Azotobacter vinelandii*, *Cyanobacterium*, and *Synechocystis*.[64−66] The reasons for the preference for dQH_2 over Q_1H_2 and Q_2H_2 are not clear but are likely a function of substrate solubility and the structural constraints of the binding pocket. In other similar redox proteins such as photosystem II and respiratory complex I, the stabilizing binding energy is provided by hydrophobic interactions between the alkenyl/aliphatic tail of the quinone and the protein pocket.[67−69] Different quinone molecules have differing degrees of mobility in the aliphatic tail, leading to differential binding and hydrophilicity in solution. The cause for the high affinity of *M. tuberculosis* cyt *bd* (19.25 μM) compared to *E. coli* (85 μM) is also uncertain but may be related to the differing sizes of the Q-loops of these enzymes.[70−72] Indeed, despite belonging to the short Q-loop family, recent cryo-EM structures found that cyt *bd* from *M. smegmatis* [73] and *M. tuberculosis* [50] had Q-loops more similar in structure to the previously identified long Q-loop *E. coli* structure. Interestingly, both structures do not contain accessory units as found in other organisms, such as CydX or CydS, and the Q-loop contains a structurally important cysteine bridge. In addition, during the course of their experiments, both teams attempted to produce structures bound to the inhibitor aurachin D that resulted in poor densities in the Q-loop, suggesting the highly flexible nature of this region. The non-Michaelis−Menten kinetics demonstrated for Q_2H_2 at first glance appears atypical but there is a precedent for this observation in the studies of *E. coli* cytochrome *bd*. Matsumoto et al. reported that structural studies identify that the 6-diprenyl and 3-methoxy groups of Q_2H_2 are the cause of substrate inhibition at high concentrations in *E. coli* and likely impart the same inhibitory effect at the active site of *M. tuberculosis* cyt *bd*.[74]

Further screening of our in-house library[55−58,75] successfully identified several distinct templates demonstrating varying degrees of activity against recombinant *M. tuberculosis* cyt *bd* (Table S1). While Templates 4 and 5 demonstrated reasonable potency against the recombinant enzyme, the effects of these

https://doi.org/10.1021/acsinfecdis.2c00283
ACS Infect. Dis. XXXX, XXX, XXX−XXX

compounds against *M. tuberculosis* were limited and as such we suggest that these linkerless pyridyl and pyrazole compounds are not suitable templates for further development. From the remaining three templates identified, it was discovered that bisaryl side chains conferred greater potency against cyt *bd* than the 2-arylamine compounds of Template 2 but diminished efficacy against *M. tuberculosis*. Template 2 compounds are also more potent against cyt *bd* than the pyridyl oxygen-linked quinolones of Template 1. In both cases, the reasons for these observations are likely a consequence of the increased steric bulk and lipophilicity of the compounds in Templates 1 and 3. The described templates exemplified by the front-runner inhibitor CK-2-63 represent the first-in-class cyt *bd* inhibitors (patent WO2017103615A1) that display tractable features for onward development. In a recent study, a putative *M. tuberculosis* cyt *bd* inhibitor ND-011992 has been described that is also based on the quinazoline core.[76,77] ND-011992 and the 2-aryl-quinolone inhibitors described in this study expand the panel of cyt *bd* inhibitors from the classic quinol analogue aurachin D.[78] However, while aurachin D has been observed to inhibit cyt *bd* from Mycobacterium spp.,[79] the observation that the mycobacterial membrane is impermeable to aurachin D,[79,80] as well as the reported lack of selective toxicity,[81,82] severely limits the developability of aurachin D compared to ND-011992 and the 2-aryl-quinolone inhibitors described herein. Further putative cytochrome bd inhibitors have recently been described; however, the evidence supporting inhibition and selectivity of cyt bd is currently limited: these compounds include MQL-H2,[83] *N*-(4-(*tert*-butyl)phenethyl)thieno[3,2-*d*]pyrimidin-4-amine,[84] and the 4-quinolinone antibacterial compounds listed in the Janssen Sciences patents WO 2021/063914 A1 and WO 2021/063915 A1. We also note that chemotypes similar to those presented here have previously been reported in the literature, such as SCR0911,[14] and it will be of interest in future studies to determine whether there are further quinolone-based inhibitors that have selectivity for cyt bd or indeed that have multiple targets owing to the privileged quinolone core, e.g., ref 85.

The cellular bioenergetic consequence of cyt *bd* inhibition by the front-runner inhibitor CK-2-63 was assessed by measurement of O_2 consumption in *M. smegmatis*. Baseline respiration parameters were confirmed using classic respiratory chain inhibitors (Seahorse assay, Figure 6A). The cyt *bd* inhibitor CK-2-63 was shown to partially inhibit O_2 consumption, though only at very high concentrations (Figure 6B). In contrast, the cyt *bcc-aa*$_3$ complex inhibitor Q203 and the ATP synthase inhibitor BDQ were shown to elicit a concentration-dependent inhibition of O_2 consumption up to the maximum basal respiration range. Significantly, the combination of a fixed concentration (3.5 μM) of CK-2-63 resulted in the potentiation of the inhibitory effect of both Q203 and BDQ across their respective concentration ranges (Figure 6C,D). Similarly, the putative cyt *bd* inhibitor ND-011992 was also recently described to enhance the inhibition of respiration of Q203 in *Mycobacterium bovis*.[77] These observations provide support that given the inherent redundancy of the mycobacterial respiratory chain, targeting multiple components of both terminal branches with small-molecule inhibitors results in enhanced inhibition at the functional level of respiration.

The pharmacological effect of inhibiting cyt *bd* was next explored by determining the effect on *M. tuberculosis* growth suppression. Initial studies using the standard 5-day alamar blue assay showed that the identified 2-aryl-quinolone inhibitors suppressed growth with measured half-maximal inhibitory concentration (IC_{50}) values as low as 0.27 μM (Table S5). Cognizant of the reported ability of *M. tuberculosis* to metabolically mediate antibiotic persistence,[86] MGIT experiments were undertaken to monitor *M. tuberculosis* growth for up to 44 days in the presence of inhibitors. Notably, addition of CK-2-63 monotherapy resulted in modest *M. tuberculosis* growth suppression measured as an increase in the time to positivity (TtP) relative to untreated controls with some combinations reaching comparable levels to the positive control isoniazid (Figure 7). This observation is consistent with previous molecular gene disruption studies showing that cyt *bd* is nonessential for growth when grown under *in vitro* laboratory conditions.[26,27] Of interest, monotherapy with equipotent concentrations of either the cyt *bcc-aa*$_3$ complex inhibitors Q203, lansoprazole, and AWE402 or the ATP synthase inhibitor BDQ also failed to completely suppress growth (Figure 7). Significantly, double combination therapies of CK-2-63 with cyt *bcc-aa*$_3$ inhibitors or with BDQ resulted in large increases in TtP (Figure 7). Moreover, triple combination therapies, consisting of cyt *bcc*, ATP synthase, and cyt *bd* inhibitors led to maximum measurable increases in TtP (44 days), matching the isoniazid positive control.

To further investigate the pharmacodynamic (PD) effect of inhibiting cyt *bd*, time-kill kinetic experiments were undertaken. 2-Aryl-quinolone inhibitors, added at equipotent concentrations (5× alamar blue 5-day growth suppression assay IC_{90} value), displayed a net bacteriostatic phenotype against *M. tuberculosis* (Figure 4). Similarly, Q203 also displayed a net bacteriostatic phenotype (Figure 8), consistent with the bacteriostatic phenotype that has been observed following inhibition by Q203 and other cytochrome *bcc-aa*$_3$ supercomplex inhibitors in previous studies.[26,77,87,88] However, significantly, combination treatment of *M. tuberculosis* with CK-2-63 and Q203 resulted in a bactericidal phenotype analogous to that seen for ethambutol and streptomycin (Figure 8). In a recent study, combination therapy of Q203 with the putative cyt *bd* inhibitor ND-01192 was also shown to result in a bactericidal phenotype against *M. tuberculosis*.[77] The switch from a bacteriostatic to a bactericidal phenotype when Q203 and cyt *bd* inhibitors are combined further supports the rationality of a combination strategy that targets both terminal branches of the *M. tuberculosis* respiratory pathway. Furthermore, CK-2-63 was also observed to enhance the bactericidal activity of suboptimal concentrations of BDQ (Figure 8). BDQ consistently (n = 3) showed a bactericidal effect for 14 days followed by a rebound of Mtb growth, likely due to metabolism changes as previously reported.[89] The addition of CK-2-63 prevented this rebound even at suboptimal concentrations (Figure 8). Kill-curve kinetics for BDQ were undertaken across the pharmacological range of BDQ, allowing the determination of the exposure effect relationship that can be parameterized to an E_{max} model, where the EC_{50} is the concentration required to achieve half of the maximal kill rate.[90] These analyses indicate that a combination of a fixed concentration of CK-2-63 (3.5 μM) results in a >3-fold enhancement in the EC_{50} of BDQ (Figure S5). This observation provides support that a cyt *bd* inhibitor combination with BDQ has the potential to significantly improve the pharmacokinetic/pharmacodynamic (PK/PD) indices related to efficacy as well as increasing the therapeutic

https://doi.org/10.1021/acsinfecdis.2c00283
ACS Infect. Dis. XXXX, XXX, XXX−XXX

index, thereby giving rise to the potential of optimized dosing that reduces the concentration-dependent side effects associated with BDQ, such as prolonged QT intervals.[91]

The *in vivo* potential of a cyt *bd* inhibitor-based combination treatment was assessed using both acute and chronic inbred mouse models of TB infection. Combination treatment of CK-2-63 with Q203, in either acute or chronic models failed to significantly reduce *M. tuberculosis* in the lungs (Figure 9). However, treatment with Q203 to mice infected with an *M. tuberculosis* mutant in which *cydA* is inactivated by a transposon insertion resulted in a reduction in the bacterial burden in the lungs (Figure 9). While the *in vivo* PK assessment of total systemic CK-2-63 exposure was ostensibly favorable (i.e., C_{max} 12.7 μg mL^{-1} at 100 mg kg^{-1}, Figure 10 and Table S6), the high plasma protein binding (>99.9% for 1 μM and 99.7% for 10 μM CK-2-63) would suggest that the available unbound drug concentration at the target site to be considerably lower (Figure 10). This potential explanation, for the lack of efficacy of CK-2-63 and Q203 combinations seen in the *in vivo* models was investigated by repeating the MGIT growth suppression assays in the presence of human serum. Significantly, following the addition of 10% (v/v) human serum, all treatments exhibited lower times to positivity, including the previously successful dual and triple combinations (Figure 11). These experiments support the interpretation that insufficient exposure of unbound CK-2-63 concentration at the target site is most likely responsible for the lack of *in vivo* efficacy. Poor solubility, high lipophilicity, and high PPM are a feature of many newly developed ETC inhibitors that mimic ubiquinone and addressing this shortcoming will be critical for future drug development efforts if a cyt *bd* inhibitor-based drug combination is to become a clinically tractable therapeutic strategy.[92−94]

In conclusion, this study reports the first characterization of cytochrome *bd*, the terminal oxidase of the branched respiratory chain of *M. tuberculosis*. A new series of cyt *bd* 2-aryl-quinolone inhibitors was identified displaying potent (nM) enzymatic inhibitory activity with predicted binding to a cleft in close proximity to the catalytically important Q-loop and a heme prosthetic group. *In vitro* drug characterization provides proof-of-concept evidence that combination treatments consisting of inhibitors to both terminal branches of the respiratory chain exhibit enhanced pharmacodynamic features that warrant further consideration toward the development of new combination strategies for the treatment of TB.

METHODS

Cloning and Heterologous Expression of *M. tuberculosis* cyt *bd*. The *cydABDC* operon was PCR amplified as a 5.9 kb fragment from *M. tuberculosis* genomic DNA using *Pfx* DNA polymerase (Invitrogen). The forward and reverse primers for this reaction were 5′-CCG GAG ATG ACA GAT GAA TGT CGT CG-3′ (Fw) and 5′-GGC GTT ACG TGC TGA TAT CGA TGA CTC AGG 3′ (Rev). The resultant fragment was subcloned to pUC19 and the sequence verified by automated DNA sequencing.

Heterologous Expression and Purification of *M. tuberculosis* Cytochrome *bd*. To facilitate heterologous expression, the pUC19-*cydABDC* construct (pTMA) was transformed into the *E. coli* cytochrome bo_3/*bd*-I knockout strain ML16 (Δ*recA*, Δ*cydAB*, Δ*cyoABCDE*::Cm^r), generously provided by (Prof. R. Gennis, University of Illinois). ML16 is a derivative of *E. coli* C43 (DE3) (genotype F$^-$*ompT gal hsdS*$_B$ (r_B-m_B-) *dcm lon* λDE3).[95] Successful transformants (TML16) were cultured in selective semi-anaerobic conditions (O_2-limited); 375 mL of Luria-Bertani (LB) broth (Formedium, U.K.) in 500 mL flasks containing 100 μg·mL^{-1} of ampicillin and 2.5 μg·mL^{-1} of chloramphenicol, sealed with a rubber plug with a head−space ratio of 0.5. Isopropyl-β-D-1-thiogalactopyranoside (IPTG) was added at the time of culture inoculation to 1 mM final concentration (Sigma-Aldrich). Cultures were incubated at 37 °C in a shaking incubator at 200 rpm for 19 h. As controls, untransformed BL21 (DE3) pLysS and untransformed ML16 cells were cultured under the same conditions.

Cells were harvested by centrifugation at 4000*g* for 10 min. Membrane preparations were performed as per Fisher et al. and resulted in highly viscous pellets.[96] These were collected and resuspended with the aid of a Potter homogenizer in 2 mL of 50 mM potassium phosphate and 2 mM ethylenediaminetetraacetic acid (EDTA) (pH 7.5) per liter of original culture volume. Glycerol was added to a final concentration of 10% (v/v) and the membrane suspensions stored at −80 °C.

Growth Analysis. Growth was monitored by measuring the optical density (OD) at 600 nm using Thermo Spectronic (Genesys, U.K.) over 60 h using the growth conditions described above. As per Karakashev et al., resazurin (a redox indicator) was added to the media to a final concentration of 0.0002% (w/v) to monitor the respiratory state of the cells during growth.[97]

Initial Spectroscopic Analysis of *M. tuberculosis* cyt *bd*. Initial spectra (500−700 nm) of freshly prepared membrane preparations were recorded using a Cary 300 Bio UV/visible spectrophotometer (Varian, U.K.). Assays of total volume 700 μL were performed using 200 μL of crude recombinant membranes suspended in 500 μL of 50 mM potassium phosphate (KPi), 2 mM EDTA, pH 7.5 buffer. For the generation of fully oxidized spectra, potassium hexacyanoferrate(III) was added, while sodium dithionite was added to produce reduced spectra. A difference spectrum was generated by subtracting the oxidized spectrum from the reduced spectrum.

Steady-State Assays and Inhibitor Studies of Recombinant *M. tuberculosis* cyt *bd*. Steady-state recombinant *M. tuberculosisbd* decylubiquinol oxidase activity was monitored spectrophotometrically at 283 nm in a 1 cm pathlength quartz cuvette. Assays (final volume 700 μL) were performed in an air-saturated reaction buffer consisting of 50 mM potassium phosphate (pH 7.5) and 2 mM EDTA. Crude recombinant membranes were added to a final protein concentration of ∼3 μg·mL^{-1}. The reaction was initiated by the addition of 50 μM quinol (either decylubiquinol, ubiquinol-1, or ubiquinol-2) from a 15 mM stock solution prepared as previously described.[98] Initial rates of quinol oxidation (decylubiquinol and ubiquinol-1) were fitted as the Michaelis−Menten function, while a modified *ping−pongbi−bi* mechanism was used for ubiquinol-2 oxidation as previously described.[74] All assays were performed at ambient temperatures. Inhibitors were added prior to reaction initiation and DMSO maintained below 1%. IC_{50} values were calculated from plots of log dose vs oxidation rate. The quinol oxidation rate was fitted to a four-parameter logistic function using Origin 8.5 (OriginLab Corp.), the and specific catalytic activity (μmol·min^{-1}·mg^{-1}) was calculated using ε_{283} = 8.1 mM^{-1}·cm^{-1}.

Modeling Inhibitors of Cytochrome *bd*. CK-2-63 and aurachin D were built using Spartan18 (https://www.wavefun.

https://doi.org/10.1021/acsinfecdis.2c00283
ACS Infect. Dis. XXXX, XXX, XXX−XXX

com) and energy minimized using the Merck molecular forcefield. GOLD 5.2 (CCDC Software)[99] was used to dock CK-2-63 and aurachin D, with the binding site of the Cryo-EM structure of the cytochrome bd oxidase from *M. tuberculosis* defined as any amino acid residue within 6 Å of menaquinone-9. A genetic algorithm with ChemPLP as the fitness function[59] was used to generate 10 binding modes per ligand. Protons were added to the protein. Default settings were retained for the "ligand flexibility" and "fitness and search" options; however, "GA settings" were changed to 200%. Figures were produced using PyMOL V1.3. Noncovalent contacts were analyzed with ViewContacts software.[100]

Production of Quinolone-Based Cytochrome *bd* Inhibitors. All compounds were from an in-house quinolone-based chemical library. The production of these compounds are described previously.[13,55−58,75]

Concentration- and Time-Dependent Drug Susceptibility Testing. For drug susceptibility testing, aerobic and hypoxic cultures of *M. tuberculosis* strain H37Rv were cultured as previously described.[9] IC_{50} data for aerobic cultures were determined using the microplate alamar blue assay (MABA) derived by Hartkoorn et al., while the modified MABA method described by Warman et al. was utilized for hypoxic studies.[9,101]

Time-kill studies were carried out using mid-log phase *M. tuberculosis* H37Rv cultures diluted to approximately 1×10^7 CFU mL^{-1} as previously described.[9] Drugs were present at final concentrations of $5xIC_{90}$, as determined from preceding *M. tuberculosis* drug susceptibility assays. Colony-forming units per milliliter were determined by plating to solid media and plotted against time to determine time-kill kinetics.

The data from time-kill studies were analyzed using the individual estimation method in ADAPT5, with a weighted least-square solution of the data. The net *M. tuberculosis* growth rate was determined by fitting individual control data. The growth rate of the mycobacteria was then fixed and the effect of different compounds in reducing the growth rate of the mycobacteria was assessed using the following equation

$$\frac{dN}{dt} = N^*\left(K_{growth}\cdot\left(1 - \frac{N}{POPMAX}\right) - K_{kill}\right)$$

where N is the absolute number of mycobacteria in the experiment, K_{growth} is a fixed growth rate of bacteria based on control data, POPMAX is the capacity limiting factor of mycobacteria, and K_{kill} is the effect of a drug on reducing the growth rate of bacteria.

Statistical Analysis and Data Visualization. Concentration-kill rate in vitro data were fitted using a four-parameter sigmoidal model according to eq 1

$$\text{kill rate } (h^{-1}) = \frac{E_{max}\ (h^{-1})\cdot \text{concn}^{\,h}\ (nM)}{EC_{50}{}^{h}\ (nM) + \text{concn}^{\,h}\ (nM)} \quad (1)$$

where E_{max} is the maximal kill rate that can be achieved, EC_{50} is the concentration required to achieve 50% of the maximal kill rate, and h is the hill slope that describes the steepness of the concentration−effect relationship. This was analyzed using Graphpad Prism 7.0.

Pharmacokinetic profiles were visualized using R 3.6.3 and AUC calculated using a trapezoidal method. C_{max} was reported as the highest observed concentration. These analyses were not attempted for blood profiles as they only capture trough concentrations.

Toxicity Studies. Activities of *M. tuberculosisbd* inhibitors against bovine cytochrome bc_1 were determined spectrophotometrically as a function of cytochrome *c* reduction as per Biagini et al. using Keilin−Hartree particles.[102,103] Inhibitors were added prior to reaction initiation with 50 μM decylubiquinol and IC_{50} values determined as per enzyme inhibition studies. Cellular toxicities were determined as previously described.[9]

Oxygen Consumption Assays. *M. smegmatis* (ATCC 19420) cultures were grown using 7H9 media (produced as suggested by the manufacturer, Sigma-Aldrich) using a 1:100 inoculation every 3−4 days. Cells were incubated at 37 °C, 170 rpm. Cells were prepared for the assay by harvesting after 72 h growth and centrifuging at 5000*g* for 15 min at 4 °C (JLA 16.250 rotor, Beckman Avanti J-25 Centrifuge). Centrifuged cells were washed with filtered potassium phosphate (KPi) buffer (K_2HPO_4 + KH_2PO_4, Sigma-Aldrich) and then concentrated to an OD_{600} = 3 by centrifugation and resuspension in fresh 7H9. Cells were stored at −20 °C until required. 1 mL (CFU mL^{-1} = 7.5×10^6) assays were conducted using a Hansatech Oxytherm+ oxygen electrode at 37 °C, 100% stirring. The 100% oxygen consumption rate was found for each assay using the rate achieved after the addition of 10 mM glucose. Once a steady oxygen rate was achieved, ETC inhibitors were sequentially added every 3 min to achieve these ranges: CK-2-63 (20−200 μM), BDQ (1−56 nM), and Q203 (10−110 nM). Combinations were assessed using the same ranges with the addition of CK-2-63 (3.5 μM) that was administered at the same time as the first drug addition. Rates were recorded from 2 min after each drug addition for 1 min. The results were analyzed using Hansatech Oxytrace software.

Time-to-Positivity Determination. *M. tuberculosis* strain H37Rv was cultured to mid-log phase as previously described.[9,61] BD MGIT (Mycobacteria Growth Indicator Tubes) 4 mL tubes where used according to manufacturer instructions (BD, U.K.). Briefly, tubes are inoculated with *M. tuberculosis* cells for a final concentration of 1.3×10^5 CFU mL^{-1}. Using previously calculated IC_{50} values, compounds were added to reach concentrations at $5 \times IC_{50}$ values for all compounds in isolation and in combinations. Tubes were incubated at 37 °C for 56 days or until positivity was reached. Positivity was measured using a MicroMGIT Fluorescence Reader (BD, U.K.). The day at which a tube gave a positive reading (≥14 afu) was determined as the time to positivity (TTP). Isoniazid was used as a positive control, while *M. tuberculosis* with and without DMSO were used as negative controls. All tubes were made in duplicate and the results averaged. The results were plotted using Prism 5 (GraphPad software). For serum-binding experiments, FBS (Gibco), Middlebrook 7H9 broth (BD diagnostics), and PBS (Gibco) were sourced from relevant suppliers. Human serum was obtained using blood donated by patients from the haemochromatosis clinic at the Royal Hospital, Liverpool. The blood was collected from patients using blood bags containing no anticoagulant. For our experiments, serum was pooled from approximately 10−15 patients.

Time-Kill Kinetics. *M. tuberculosis* H37Rv cultures at OD_{600} = 0.3 were incubated with drugs at varying concentrations. Cultures were aliquoted into 1.5 mL bijous, treated with drugs at $5xIC_{90}$ for all compounds except Q203 (400 nM) and CK-2-63 (3.5 or 35 μM), and incubated at 37 °C for 0, 3, 5, 7, 10, 14, 17, or 21 days. After the determined length of time, 1 mL aliquots were removed from each bijou

https://doi.org/10.1021/acsinfecdis.2c00283
ACS Infect. Dis. XXXX, XXX, XXX−XXX

and centrifuged at 14,000 rpm for 10 min. The supernatant was removed and the pellet resuspended in fresh 7H9 media to remove the extracellular drug. Serial dilutions were produced for each condition from 10^0 (neat) to 10^{-8}. The dilutions were spotted onto 7H11 agar plates with three drops of 20 μL per dilution. Plates were inverted and incubated at 37 °C until countable colonies were observed.

Efficacy in Mouse Models of TB. Initially, the PK of CK-2-63 was studied in female BALB/c mice following either single dose intravenous administration (IV) via tail vein of 3 mg kg^{-1} CK-2-63 or oral gavage (PO) of 20 mg kg^{-1} CK-2-63 formulated as solutions in 80% PEG200 to fed mice, or single dose PO administration of 100 mg kg^{-1} CK-2-63 formulated in 100% PEG200 to fasted mice, with food returned 4 h post-dose. The IV formulation was filtered through a 0.22 μm filter before dosing.

For further studies, mouse models were challenged with CK-2-63, Q203, or the positive controls rifampicin or isoniazid. Rifampicin and isoniazid were dissolved in distilled water every week. Q203 was formulated in 20% (w/w) TPGS [D-α tocopheryl poly(ethylene glycol) 1000 succinate] solution each week. CK-2-63 was prepared in 80% PEG200/20% water (v/v) each week. Dosing was once daily, by gavage, administered either 5 days/wk (Mon−Fri) (QD) or 3 days/wk (Mon, Wed, Fri) (QOD).

Blood samples were collected into tubes containing 0.5 M K2EDTA as the anticoagulant, via serial bleeding from three mice per time point, over the course of 32 h post-dose for IV administration, 96 h post-dose for PO 20 mg kg^{-1}, and 72 h post-dose for PO 100 mg kg^{-1} routes, using two sets of mice per route. Plasma was prepared via centrifugation (4 °C and 3000g) within 30 min of collection, quick frozen on dry ice, and stored frozen (−70 °C) until analysis. Plasma concentrations were determined by liquid chromatography-mass spectrometry (LC-MS)/MS analysis. Noncompartmental PK analysis was performed with Phoenix WinNonlin 6.3 software using composite data.

For the chronic mouse infection model, female BALB/c mice were infected via the aerosol route with ∼2 $\log_{10}$ colony-forming units (CFU) of *M. tuberculosis* H37Rv. Treatment started 4 weeks later (day 0). Mice were sacrificed the day after infection and on day 0 to determine the number of CFU implanted and the number present at the start of the treatment, respectively.

For the acute mouse infection model, female BALB/c mice were infected via the aerosol route with ∼4 $\log_{10}$ CFU of one of the following: *M. tuberculosis* H37Rv, *M. tuberculosis* CDC1551, or an isogenic *cydA* loss-of-function mutant[63] in which the Himar1 transposon is inserted at nt682 in the *cydA* (Rv1623c) gene in the CDC1551 background (Strain: JHU1623c-682).[63] Treatment started 3 days later (day 0).

CK-2-63 concentrations in whole blood were determined predose and 5, 24, and 45 h after the first dose and after the Wednesday dose during the 4th week of treatment in the chronic infection model. The same three mice in each group were sampled at each time point. Blood was sampled from the tail vein and collected into tubes containing EDTA. Measurement of CK-2-63 concentrations was determined by a validated LC/MS method at Alliance Pharma (a contract research organization based in Wiltshire, U.K.). Efficacy was assessed by quantifying lung CFU after 4 weeks of treatment. At each time point, mice were sacrificed, lungs were removed aseptically, and the right lung was homogenized. Serial 10-fold dilutions of the lung homogenates were plated on 7H11 agar supplemented with 0.4% activated charcoal. Final CFU counts were determined after 6 weeks of incubation.

Animal studies were carried out in adherence to all relevant US national guidelines for working with animals. Johns Hopkins University is registered with the USDA to conduct animal research. The work relating to antitubercular *in vivo* efficacy was approved by the Animal Care and Use Committee of Johns Hopkins University.

■ ASSOCIATED CONTENT

Supporting Information

The Supporting Information is available free of charge at https://pubs.acs.org/doi/10.1021/acsinfecdis.2c00283.

> Steady-state kinetics of purified cytochrome *bd* with quinol molecules; growth inhibition profiles of H37Rv against a quinolone library; inhibitory kinetics of cytochrome *bd* inhibitors; time-dependent killing of selected quinolone inhibitors in aerobic and anaerobic conditions; bovine cytochrome bc_1 and human cell counter screens against lead compounds; AUC and C_{max} values in the plasma of BALB/c mice; overexpression of cytochrome *bd* in *E. coli* cells; effects of detergents and pH on purified cytochrome *bd* catalytic activity; linear and nonlinear kinetics of quinolone inhibitors; sensitivity of H37Rv to quinolone inhibitors; and time-kill relationship of bedaquiline and CK-2-63 (PDF)

■ AUTHOR INFORMATION

Corresponding Author

Giancarlo A. Biagini − *Centre for Drugs and Diagnostics, Department of Tropical Infectious Diseases, Liverpool School of Tropical Medicine, Liverpool L3 5QA, U.K.*; Phone: +44 (0)151 7053151; Email: giancarlo.biagini@lstmed.ac.uk

Authors

Laura N. Jeffreys − *Centre for Drugs and Diagnostics, Department of Tropical Infectious Diseases, Liverpool School of Tropical Medicine, Liverpool L3 5QA, U.K.*; orcid.org/0000-0002-0607-6116

Alison Ardrey − *Centre for Drugs and Diagnostics, Department of Tropical Infectious Diseases, Liverpool School of Tropical Medicine, Liverpool L3 5QA, U.K.*

Taghreed A. Hafiz − *Centre for Drugs and Diagnostics, Department of Tropical Infectious Diseases, Liverpool School of Tropical Medicine, Liverpool L3 5QA, U.K.*

Lauri-Anne Dyer − *Centre for Drugs and Diagnostics, Department of Tropical Infectious Diseases, Liverpool School of Tropical Medicine, Liverpool L3 5QA, U.K.*

Ashley J. Warman − *Centre for Drugs and Diagnostics, Department of Tropical Infectious Diseases, Liverpool School of Tropical Medicine, Liverpool L3 5QA, U.K.*

Nada Mosallam − *Department of Chemistry, University of Liverpool, Liverpool L69 7ZD, U.K.*

Gemma L. Nixon − *Department of Chemistry, University of Liverpool, Liverpool L69 7ZD, U.K.*; orcid.org/0000-0002-9730-0960

Nicholas E. Fisher − *Centre for Drugs and Diagnostics, Department of Tropical Infectious Diseases, Liverpool School of Tropical Medicine, Liverpool L3 5QA, U.K.*

W. David Hong − *Department of Chemistry, University of Liverpool, Liverpool L69 7ZD, U.K.;* orcid.org/0000-0002-0030-3007
Suet C. Leung − *Department of Chemistry, University of Liverpool, Liverpool L69 7ZD, U.K.*
Ghaith Aljayyoussi − *Centre for Drugs and Diagnostics, Department of Tropical Infectious Diseases, Liverpool School of Tropical Medicine, Liverpool L3 5QA, U.K.*
Jaclyn Bibby − *Department of Chemistry, University of Liverpool, Liverpool L69 7ZD, U.K.*
Deepak V. Almeida − *Center for Tuberculosis Research, Johns Hopkins University School of Medicine, Baltimore, Maryland 21205, United States*
Paul J. Converse − *Center for Tuberculosis Research, Johns Hopkins University School of Medicine, Baltimore, Maryland 21205, United States*
Nader Fotouhi − *Global Alliance for TB Drug Development, New York, New York 10005, United States*
Neil G. Berry − *Department of Chemistry, University of Liverpool, Liverpool L69 7ZD, U.K.*
Eric L. Nuermberger − *Center for Tuberculosis Research, Johns Hopkins University School of Medicine, Baltimore, Maryland 21205, United States*
Anna M. Upton − *Global Alliance for TB Drug Development, New York, New York 10005, United States; Evotec (US) Inc., Princeton, New Jersey 08540, United States;* orcid.org/0000-0002-9522-1230
Paul M. O'Neill − *Department of Chemistry, University of Liverpool, Liverpool L69 7ZD, U.K.;* orcid.org/0000-0003-4338-0317
Stephen A. Ward − *Centre for Drugs and Diagnostics, Department of Tropical Infectious Diseases, Liverpool School of Tropical Medicine, Liverpool L3 5QA, U.K.*

Complete contact information is available at: https://pubs.acs.org/10.1021/acsinfecdis.2c00283

Author Contributions

G.A.B. conceived the study; G.A.B., S.A.W., P.O.N., A.U., E.N., and N.F. directed the project. All authors contributed to the experimental design and implementation of the research; L.N.J., A.A., T.A.H., A.J.W., N.M., G.L.N., S.C.L. N.E.F., G.A., J.B., D.V.A., P.J.C., and N.B., performed the experiments and contributed to the analysis and interpretation of the results. G.A.B. and L.N.J. drafted the initial manuscript with contributions from all authors.

Notes

The authors declare no competing financial interest.

■ ACKNOWLEDGMENTS

The authors are grateful to Professor Robert Gennis, University of Illinois, and Dr. Martijn Bekker, University of Amsterdam, for their generous donations of biological materials. This work was supported by grants from the Wellcome Trust, the National Institute of Health Research (NIHR, BRC Liverpool), the Leverhulme Trust, and the Medical Research Council (MR/S00467X/1; MC_PC_17225; MR/N028376/1). T.H. was supported through a Ph.D. scholarship from King Saud University, Saudi Arabia.

■ REFERENCES

(1) Bagcchi, S. Dismal global tuberculosis situation due to COVID-19. *Lancet Infect. Dis.* **2021**, *21*, 1636.
(2) Chakaya, J.; Khan, M.; Ntoumi, F.; Aklillu, E.; Fatima, R.; Mwaba, P.; Kapata, N.; Mfinanga, S.; Hasnain, S. E.; Katoto, P.; Bulabula, A. N. H.; Sam-Agudu, N. A.; Nachega, J. B.; Tiberi, S.; McHugh, T. D.; Abubakar, I.; Zumla, A. Global Tuberculosis Report 2020—Reflections on the Global TB burden, treatment and prevention efforts. *Int. J. Infect. Dis.* **2021**, *113*, S7−S12.
(3) Weinstein, E. A.; Yano, T.; Li, L. S.; Avarbock, D.; Avarbock, A.; Helm, D.; McColm, A. A.; Duncan, K.; Lonsdale, J. T.; Rubin, H. Inhibitors of type II NADH:menaquinone oxidoreductase represent a class of antitubercular drugs. *Proc. Natl. Acad. Sci. U.S.A.* **2005**, *102*, 4548−4553.
(4) Koul, A.; Dendouga, N.; Vergauwen, K.; Molenberghs, B.; Vranckx, L.; Willebrords, R.; Ristic, Z.; Lill, H.; Dorange, I.; Guillemont, J.; Bald, D.; Andries, K. Diarylquinolines target subunit c of mycobacterial ATP synthase. *Nat. Chem. Biol.* **2007**, *3*, 323−324.
(5) Koul, A.; Vranckx, L.; Dendouga, N.; Balemans, W.; Van den Wyngaert, I.; Vergauwen, K.; Gohlmann, H. W.; Willebrords, R.; Poncelet, A.; Guillemont, J.; Bald, D.; Andries, K. Diarylquinolines are bactericidal for dormant mycobacteria as a result of disturbed ATP homeostasis. *J. Biol. Chem.* **2008**, *283*, 25273−25280.
(6) Haagsma, A. C.; Abdillahi-Ibrahim, R.; Wagner, M. J.; Krab, K.; Vergauwen, K.; Guillemont, J.; Andries, K.; Lill, H.; Koul, A.; Bald, D. Selectivity of TMC207 towards mycobacterial ATP synthase compared with that towards the eukaryotic homologue. *Antimicrob. Agents Chemother.* **2009**, *53*, 1290−1292.
(7) Rao, S. P. S.; Alonso, S.; Rand, L.; Dick, T.; Pethe, K. The protonmotive force is required for maintaining ATP homeostasis and viability of hypoxic, nonreplicating *Mycobacterium tuberculosis*. *Proc. Natl. Acad. Sci. U.S.A.* **2008**, *105*, 11945−11950.
(8) Diacon, A. H.; Pym, A.; Grobusch, M.; Patientia, R.; Rustomjee, R.; Page-Shipp, L.; Pistorius, C.; Krause, R.; Bogoshi, M.; Churchyard, G.; Venter, A.; Allen, J.; Palomino, J. C.; De Marez, T.; van Heeswijk, R. P.; Lounis, N.; Meyvisch, P.; Verbeeck, J.; Parys, W.; de Beule, K.; Andries, K.; Mc Neeley, D. F. The diarylquinoline TMC207 for multidrug-resistant tuberculosis. *N. Engl. J. Med.* **2009**, *360*, 2397−2405.
(9) Warman, A. J.; Rito, T. S.; Fisher, N. E.; Moss, D. M.; Berry, N. G.; O'Neill, P. M.; Ward, S. A.; Biagini, G. A. Antitubercular pharmacodynamics of phenothiazines. *J. Antimicrob. Chemother.* **2013**, *68*, 869−880.
(10) Bloemberg, G. V.; Keller, P. M.; Stucki, D.; Trauner, A.; Borrell, S.; Latshang, T.; Coscolla, M.; Rothe, T.; Homke, R.; Ritter, C.; Feldmann, J.; Schulthess, B.; Gagneux, S.; Bottger, E. C. Acquired Resistance to Bedaquiline and Delamanid in Therapy for Tuberculosis. *N. Engl. J. Med.* **2015**, *373*, 1986−1988.
(11) Tantry, S. J.; Markad, S. D.; Shinde, V.; Bhat, J.; Balakrishnan, G.; Gupta, A. K.; Ambady, A.; Raichurkar, A.; Kedari, C.; Sharma, S.; Mudugal, N. V.; Narayan, A.; Naveen Kumar, C. N.; Nanduri, R.; Bharath, S.; Reddy, J.; Panduga, V.; Prabhakar, K. R.; Kandaswamy, K.; Saralaya, R.; Kaur, P.; Dinesh, N.; Guptha, S.; Rich, K.; Murray, D.; Plant, H.; Preston, M.; Ashton, H.; Plant, D.; Walsh, J.; Alcock, P.; Naylor, K.; Collier, M.; Whiteaker, J.; McLaughlin, R. E.; Mallya, M.; Panda, M.; Rudrapatna, S.; Ramachandran, V.; Shandil, R.; Sambandamurthy, V. K.; Mdluli, K.; Cooper, C. B.; Rubin, H.; Yano, T.; Iyer, P.; Narayanan, S.; Kavanagh, S.; Mukherjee, K.; Balasubramanian, V.; Hosagrahara, V. P.; Solapure, S.; Ravishankar, S.; Hameed, P. S. Discovery of Imidazo[1,2-a]pyridine Ethers and Squaramides as Selective and Potent Inhibitors of Mycobacterial Adenosine Triphosphate (ATP) Synthesis. *J. Med. Chem.* **2017**, *60*, 1379−1399.
(12) Mapari, M.; Bhole, R. P.; Khedekar, P. B.; Chikhale, R. V. Challenges in targeting mycobacterial ATP synthase: The known and beyond. *J. Mol. Struct.* **2022**, *1247*, No. 131331.
(13) Moraski, G. C.; Markley, L. D.; Cramer, J.; Hipskind, P. A.; Boshoff, H.; Bailey, M.; Alling, T.; Ollinger, J.; Parish, T.; Miller, M. J. Advancement of Imidazo[1,2-a]pyridines with Improved Pharmacokinetics and Nanomolar Activity Against *Mycobacterium tuberculosis*. *ACS Med. Chem. Lett.* **2013**, *4*, 675−679.

(14) Chong, S. M. S.; Manimekalai, M. S. S.; Sarathy, J. P.; Williams, Z. C.; Harold, L. K.; Cook, G. M.; Dick, T.; Pethe, K.; Bates, R. W.; Gruber, G. Antituberculosis Activity of the Antimalaria Cytochrome bcc Oxidase Inhibitor SCR0911. *ACS Infect. Dis.* **2020**, *6*, 725−737.
(15) Rybniker, J.; Vocat, A.; Sala, C.; Busso, P.; Pojer, F.; Benjak, A.; Cole, S. T. Lansoprazole is an antituberculous prodrug targeting cytochrome bc1. *Nat. Commun.* **2015**, *6*, No. 7659.
(16) de Jager, V. R.; Dawson, R.; van Niekerk, C.; Hutchings, J.; Kim, J.; Vanker, N.; van der Merwe, L.; Choi, J.; Nam, K.; Diacon, A. H. Telacebec (Q203), a New Antituberculosis Agent. *N. Engl. J. Med.* **2020**, *382*, 1280−1281.
(17) Sun, Z.; Zhang, Y. Antituberculosis activity of certain antifungal and antihelmintic drugs. *Tuberc. Lung Dis.* **1999**, *79*, 319−20.
(18) Vosátka, R.; Kratky, M.; Vinsova, J. Triclosan and its derivatives as antimycobacterial active agents. *Eur. J. Pharm. Sci.* **2018**, *114*, 318−331.
(19) Eoh, H.; Rhee, K. Y. Multifunctional essentiality of succinate metabolism in adaptation to hypoxia in *Mycobacterium tuberculosis*. *Proc. Natl. Acad. Sci. U.S.A.* **2013**, *110*, 6554−6559.
(20) Lechartier, B.; Cole, S. T. Mode of Action of Clofazimine and Combination Therapy with Benzothiazinones against *Mycobacterium tuberculosis*. *Antimicrob. Agents Chemother.* **2015**, *59*, 4457−63.
(21) Lu, P.; Asseri, A. H.; Kremer, M.; Maaskant, J.; Ummels, R.; Lill, H.; Bald, D. The anti-mycobacterial activity of the cytochrome bcc inhibitor Q203 can be enhanced by small-molecule inhibition of cytochrome bd. *Sci. Rep.* **2018**, *8*, No. 2625.
(22) Luo, M.; Zhou, W.; Patel, H.; Srivastava, A. P.; Symersky, J.; Bonar, M. M.; Faraldo-Gomez, J. D.; Liao, M.; Mueller, D. M. Bedaquiline inhibits the yeast and human mitochondrial ATP synthases. *Commun. Biol.* **2020**, *3*, No. 452.
(23) Sarathy, J. P.; Ragunathan, P.; Shin, J.; Cooper, C. B.; Upton, A. M.; Gruber, G.; Dick, T. TBAJ-876 Retains Bedaquiline's Activity against Subunits c and epsilon of *Mycobacterium tuberculosis* F-ATP Synthase. *Antimicrob. Agents Chemother.* **2019**, *63*, No. e01191-19.
(24) Xu, J.; Converse, P. J.; Upton, A. M.; Mdluli, K.; Fotouhi, N.; Nuermberger, E. L. Comparative Efficacy of the Novel Diarylquinoline TBAJ-587 and Bedaquiline against a Resistant Rv0678 Mutant in a Mouse Model of Tuberculosis. *Antimicrob. Agents Chemother.* **2021**, *65*, No. e01412-21.
(25) Griffin, J. E.; Gawronski, J. D.; DeJesus, M. A.; Ioerger, T. R.; Akerley, B. J.; Sassetti, C. M. High-resolution phenotypic profiling defines genes essential for mycobacterial growth and cholesterol catabolism. *PLoS Pathog.* **2011**, *7*, No. e1002251.
(26) Arora, K.; Ochoa-Montano, B.; Tsang, P. S.; Blundell, T. L.; Dawes, S. S.; Mizrahi, V.; Bayliss, T.; Mackenzie, C. J.; Cleghorn, L. A.; Ray, P. C.; Wyatt, P. G.; Uh, E.; Lee, J.; Barry, C. E., 3rd; Boshoff, H. I. Respiratory flexibility in response to inhibition of cytochrome C oxidase in *Mycobacterium tuberculosis*. *Antimicrob. Agents Chemother.* **2014**, *58*, 6962−6965.
(27) Berney, M.; Hartman, T. E.; Jacobs, W. R., Jr. A *Mycobacterium tuberculosis* cytochrome bd oxidase mutant is hypersensitive to bedaquiline. *mBio* **2014**, *5*, No. e01275-14.
(28) Foo, C. S.; Lupien, A.; Kienle, M.; Vocat, A.; Benjak, A.; Sommer, R.; Lamprecht, D. A.; Steyn, A. J. C.; Pethe, K.; Piton, J.; Altmann, K. H.; Cole, S. T. Arylvinylpiperazine Amides, a New Class of Potent Inhibitors Targeting QcrB of *Mycobacterium tuberculosis*. *mBio* **2018**, *9*, No. e01276-18.
(29) Kalia, N. P.; Hasenoehrl, E. J.; Ab Rahman, N. B.; Koh, V. H.; Ang, M. L. T.; Sajorda, D. R.; Hards, K.; Gruber, G.; Alonso, S.; Cook, G. M.; Berney, M.; Pethe, K. Exploiting the synthetic lethality between terminal respiratory oxidases to kill *Mycobacterium tuberculosis* and clear host infection. *Proc. Natl. Acad. Sci. U.S.A.* **2017**, *114*, 7426−7431.
(30) Osborne, J. P.; Gennis, R. B. Sequence analysis of cytochrome bd oxidase suggests a revised topology for subunit I. *Biochim. Biophys. Acta, Bioenerg.* **1999**, *1410*, 32−50.
(31) Shi, L.; Sohaskey, C. D.; Kana, B. D.; Dawes, S.; North, R. J.; Mizrahi, V.; Gennaro, M. L. Changes in energy metabolism of *Mycobacterium tuberculosis* in mouse lung and under in vitro conditions affecting aerobic respiration. *Proc. Natl. Acad. Sci. U.S.A.* **2005**, *102*, 15629−15634.
(32) Zhang-Barber, L.; Turner, A. K.; Martin, G.; Frankel, G.; Dougan, G.; Barrow, P. A. Influence of genes encoding proton-translocating enzymes on suppression of *Salmonella typhimurium* growth and colonization. *J. Bacteriol.* **1997**, *179*, 7186−7190.
(33) Juty, N. S.; Moshiri, F.; Merrick, M.; Anthony, C.; Hill, S. The *Klebsiella pneumoniae* cytochrome bd' terminal oxidase complex and its role in microaerobic nitrogen fixation. *Microbiology* **1997**, *143*, 2673−2683.
(34) Larsen, M. H.; Kallipolitis, B. H.; Christiansen, J. K.; Olsen, J. E.; Ingmer, H. The response regulator ResD modulates virulence gene expression in response to carbohydrates in *Listeria monocytogenes*. *Mol. Microbiol.* **2006**, *61*, 1622−1635.
(35) Kana, B. D.; Machowski, E. E.; Schechter, N.; Teh, J.-S.; Rubin, H.; Mizrahi, V. In *Electron Transport and Respiration in Mycobacteria*; Caister Academic Press: 32 Hewitts Lane, Wymondham Nr 18 0ja, UK, 2009; pp 35−64.
(36) Paulus, A.; Rossius, S. G.; Dijk, M.; de Vries, S. Oxoferryl-porphyrin radical catalytic intermediate in cytochrome bd oxidases protects cells from formation of reactive oxygen species. *J. Biol. Chem.* **2012**, *287*, 8830−8838.
(37) Miller, M. J.; Gennis, R. B. The purification and characterization of the cytochrome *d* terminal oxidase complex of the *Escherichia coli* aerobic respiratory chain. *J. Biol. Chem.* **1983**, *258*, 9159−9165.
(38) Junemann, S. Cytochrome bd terminal oxidase. *Biochim. Biophys. Acta, Bioenerg.* **1997**, *1321*, 107−127.
(39) Borisov, V. B.; Gennis, R. B.; Hemp, J.; Verkhovsky, M. I. The cytochrome bd respiratory oxygen reductases. *Biochim. Biophys. Acta, Bioenerg.* **2011**, *1807*, 1398−1413.
(40) Giuffrè, A.; Borisov, V. B.; Arese, M.; Sarti, P.; Forte, E. Cytochrome *bd* oxidase and bacterial tolerance to oxidative and nitrosative stress. *Biochim. Biophys. Acta, Bioenerg.* **2014**, 1178−1187.
(41) Shi, L. B.; Sohaskey, C. D.; Kana, B. D.; Dawes, S.; North, R. J.; Mizrahi, V.; Gennaro, M. L. Changes in energy metabolism of *Mycobacterium tuberculosis* in mouse lung and under in vitro conditions affecting aerobic respiration. *Proc. Natl. Acad. Sci. U.S.A.* **2005**, *102*, 15629−15634.
(42) Small, J. L.; Park, S. W.; Kana, B. D.; Ioerger, T. R.; Sacchettini, J. C.; Ehrt, S. Perturbation of cytochrome c maturation reveals adaptability of the respiratory chain in *Mycobacterium tuberculosis*. *mBio* **2013**, *4*, No. e00475-13.
(43) Borisov, V. B.; Forte, E.; Davletshin, A.; Mastronicola, D.; Sarti, P.; Giuffre, A. Cytochrome *bd* oxidase from *Escherichia coli* displays high catalase activity: An additional defense against oxidative stress. *FEBS Lett.* **2013**, *587*, 2214−2218.
(44) Parish, T.; Brown, A.*Mycobacterium: Genomics and Molecular Biology*; Caister Academic Press: Norfolk, UK, 2009.
(45) Pittman, M. S.; Robinson, H. C.; Poole, R. K. A bacterial glutathione transporter (*Escherichia coli* CydDC) exports reductant to the periplasm. *J. Biol. Chem.* **2005**, *280*, 32254−32261.
(46) Braibant, M.; Gilot, P.; Content, J. The ATP binding cassette (ABC) transport systems of *Mycobacterium tuberculosis*. *FEMS Microbiol. Rev.* **2000**, *24*, 449−67.
(47) Safarian, S.; Rajendran, C.; Muller, H.; Preu, J.; Langer, J. D.; Ovchinnikov, S.; Hirose, T.; Kusumoto, T.; Sakamoto, J.; Michel, H. Structure of a bd oxidase indicates similar mechanisms for membrane-integrated oxygen reductases. *Science* **2016**, *352*, 583−586.
(48) Theßeling, A.; Rasmussen, T.; Burschel, S.; Wohlwend, D.; Kagi, J.; Muller, R.; Bottcher, B.; Friedrich, T. Homologous bd oxidases share the same architecture but differ in mechanism. *Nat. Commun.* **2019**, *10*, No. 5138.
(49) Safarian, S.; Hahn, A.; Mills, D. J.; Radloff, M.; Eisinger, M. L.; Nikolaev, A.; Meier-Credo, J.; Melin, F.; Miyoshi, H.; Gennis, R. B.; Sakamoto, J.; Langer, J. D.; Hellwig, P.; Kuhlbrandt, W.; Michel, H. Active site rearrangement and structural divergence in prokaryotic respiratory oxidases. *Science* **2019**, *366*, 100−104.

https://doi.org/10.1021/acsinfecdis.2c00283
ACS Infect. Dis. XXXX, XXX, XXX−XXX

(50) Safarian, S.; Opel-Reading, H. K.; Wu, D.; Mehdipour, A. R.; Hards, K.; Harold, L. K.; Radloff, M.; Stewart, I.; Welsch, S.; Hummer, G.; Cook, G. M.; Krause, K. L.; Michel, H. The cryo-EM structure of the bd oxidase from M. tuberculosis reveals a unique structural framework and enables rational drug design to combat TB. *Nat. Commun.* **2021**, *12*, No. 5236.
(51) Belevich, I.; Borisov, V. B.; Zhang, J.; Yang, K.; Konstantinov, A. A.; Gennis, R. B.; Verkhovsky, M. I. Time-resolved electrometric and optical studies on cytochrome bd suggest a mechanism of electron-proton coupling in the di-heme active site. *Proc. Natl. Acad. Sci. U.S.A.* **2005**, *102*, 3657−3662.
(52) Borisov, V. B.; Siletsky, S. A.; Paiardini, A.; Hoogewijs, D.; Forte, E.; Giuffre, A.; Poole, R. K. Bacterial Oxidases of the Cytochrome bd Family: Redox Enzymes of Unique Structure, Function, and Utility As Drug Targets. *Antioxid. Redox Signaling* **2021**, *34*, 1280−1318.
(53) Voggu, L.; Schlag, S.; Biswas, R.; Rosenstein, R.; Rausch, C.; Gotz, F. Microevolution of cytochrome bd oxidase in Staphylococci and its implication in resistance to respiratory toxins released by Pseudomonas. *J. Bacteriol.* **2006**, *188*, 8079−8086.
(54) Johnson, K. A.; Menten, M. L.; Johnson, K. A.; Goody, R. S. The original Michaelis constant: translation of the 1913 Michaelis-Menten paper. *Biochemistry* **2011**, *50*, 8264−8249.
(55) Hong, W. D.; Gibbons, P. D.; Leung, S. C.; Amewu, R.; Stocks, P. A.; Stachulski, A.; Horta, P.; Cristiano, M. L. S.; Shone, A. E.; Moss, D.; Ardrey, A.; Sharma, R.; Warman, A. J.; Bedingfield, P. T. P.; Fisher, N. E.; Aljayyoussi, G.; Mead, S.; Caws, M.; Berry, N. G.; Ward, S. A.; Biagini, G. A.; O'Neill, P. M.; Nixon, G. L. Rational Design, Synthesis, and Biological Evaluation of Heterocyclic Quinolones Targeting the Respiratory Chain of *Mycobacterium tuberculosis*. *J. Med. Chem.* **2017**, *60*, 3703−3726.
(56) Pidathala, C.; Amewu, R.; Pacorel, B.; Nixon, G. L.; Gibbons, P.; Hong, W. D.; Leung, S. C.; Berry, N. G.; Sharma, R.; Stocks, P. A.; Srivastava, A.; Shone, A. E.; Charoensutthivarakul, S.; Taylor, L.; Berger, O.; Mbekeani, A.; Hill, A.; Fisher, N. E.; Warman, A. J.; Biagini, G. A.; Ward, S. A.; O'Neill, P. M. Identification, design and biological evaluation of bisaryl quinolones targeting *Plasmodium falciparum* type II NADH:quinone oxidoreductase (PfNDH2). *J. Med. Chem.* **2012**, *55*, 1831−1843.
(57) Leung, S. C.; Gibbons, P.; Amewu, R.; Nixon, G. L.; Pidathala, C.; Hong, W. D.; Pacorel, B.; Berry, N. G.; Sharma, R.; Stocks, P. A.; Srivastava, A.; Shone, A. E.; Charoensutthivarakul, S.; Taylor, L.; Berger, O.; Mbekeani, A.; Hill, A.; Fisher, N. E.; Warman, A. J.; Biagini, G. A.; Ward, S. A.; O'Neill, P. M. Identification, design and biological evaluation of heterocyclic quinolones targeting *Plasmodium falciparum* type II NADH:quinone oxidoreductase (PfNDH2). *J. Med. Chem.* **2012**, *55*, 1844−1857.
(58) David Hong, W.; Leung, S. C.; Amporndanai, K.; Davies, J.; Priestley, R. S.; Nixon, G. L.; Berry, N. G.; Samar Hasnain, S.; Antonyuk, S.; Ward, S. A.; Biagini, G. A.; O'Neill, P. M. Potent Antimalarial 2-Pyrazolyl Quinolone bc 1 (Qi) Inhibitors with Improved Drug-like Properties. *ACS Med. Chem. Lett.* **2018**, *9*, 1205−1210.
(59) Korb, O.; Stutzle, T.; Exner, T. E. Empirical scoring functions for advanced protein-ligand docking with PLANTS. *J. Chem. Inf. Model.* **2009**, *49*, 84−96.
(60) Baker, N. A.; Sept, D.; Joseph, S.; Holst, M. J.; McCammon, J. A. Electrostatics of nanosystems: application to microtubules and the ribosome. *Proc. Natl. Acad. Sci. U.S.A.* **2001**, *98*, 10037−10041.
(61) Kruuner, A.; Yates, M. D.; Drobniewski, F. A. Evaluation of MGIT 960-based antimicrobial testing and determination of critical concentrations of first- and second-line antimicrobial drugs with drug-resistant clinical strains of *Mycobacterium tuberculosis*. *J. Clin. Microbiol.* **2006**, *44*, 811−818.
(62) Vilchèze, C.; Jacobs, W. R., Jr. The Isoniazid Paradigm of Killing, Resistance, and Persistence in *Mycobacterium tuberculosis*. *J. Mol. Biol.* **2019**, *431*, 3450−3461.
(63) Lamichhane, G.; Zignol, M.; Blades, N. J.; Geiman, D. E.; Dougherty, A.; Grosset, J.; Broman, K. W.; Bishai, W. R. A postgenomic method for predicting essential genes at subsaturation levels of mutagenesis: application to *Mycobacterium tuberculosis*. *Proc. Natl. Acad. Sci. U.S.A.* **2003**, *100*, 7213−7218.
(64) Kolonay, J. F.; Moshiri, F.; Gennis, R. B.; Kaysser, T. M.; Maier, R. J. Purification and characterization of the cytochrome *bd* complex from *Azotobacter vinelandii*—Comparison to the complex from *Escherichia coli*. *J. Bacteriol.* **1994**, *176*, 4177−4181.
(65) Lorence, R. M.; Miller, M. J.; Borochov, A.; Faimanweinberg, R.; Gennis, R. B. Effects of pH and detergent on the kinetic and electrochemical properties of the purified cytochrome *d* terminal oxidase complex of *Escherichia coli*. *Biochim. Biophys. Acta, Protein Struct. Mol. Enzymol.* **1984**, *790*, 148−153.
(66) Mogi, T.; Miyoshi, H. Properties of cytochrome *bd* plastoquinol oxidase from the Cyanobacterium Synechocystis sp PCC 6803. *J. Biochem.* **2009**, *145*, 395−401.
(67) Fedor, J. G.; Jones, A. J. Y.; Di Luca, A.; Kaila, V. R. I.; Hirst, J. Correlating kinetic and structural data on ubiquinone binding and reduction by respiratory complex I. *Proc. Natl. Acad. Sci. U.S.A.* **2017**, *114*, 12737−12742.
(68) Warncke, K.; Gunner, M. R.; Braun, B. S.; Gu, L.; Yu, C. A.; Bruce, J. M.; Dutton, P. L. Influence of hydrocarbon tail structure on quinone binding and electron-transfer performance at the QA and QB sites of the photosynthetic reaction center protein. *Biochemistry* **1994**, *33*, 7830−7841.
(69) Lambreva, M. D.; Russo, D.; Polticelli, F.; Scognamiglio, V.; Antonacci, A.; Zobnina, V.; Campi, G.; Rea, G. Structure/function/dynamics of photosystem II plastoquinone binding sites. *Curr. Protein Pept. Sci.* **2014**, *15*, 285−295.
(70) Borisov, V. B.; Gennis, R. B.; Hemp, J.; Verkhovsky, M. I. The cytochrome *bd* respiratory oxygen reductases. *Biochim. Biophys. Acta, Bioenerg.* **2011**, *1807*, 1398−1413.
(71) Osborne, J. P.; Gennis, R. B. Sequence analysis of cytochrome *bd* oxidase suggests a revised topology for subunit I. *Biochim. Biophys. Acta, Bioenerg.* **1999**, *1410*, 32−50.
(72) Sakamoto, J.; Koga, E.; Mizuta, T.; Sato, C.; Noguchi, S.; Sone, N. Gene structure and quinol oxidase activity of a cytochrome *bd*-type oxidase from *Bacillus stearothermophilus*. *Biochim. Biophys. Acta, Bioenerg.* **1999**, *1411*, 147−158.
(73) Wang, W.; Gao, Y.; Tang, Y.; Zhou, X.; Lai, Y.; Zhou, S.; Zhang, Y.; Yang, X.; Liu, F.; Guddat, L. W.; Wang, Q.; Rao, Z.; Gong, H. Cryo-EM structure of mycobacterial cytochrome bd reveals two oxygen access channels. *Nat. Commun.* **2021**, *12*, No. 4621.
(74) Matsumoto, Y.; Muneyuki, E.; Fujita, D.; Sakamoto, K.; Miyoshi, H.; Yoshida, M.; Mogi, T. Kinetic mechanism of quinol oxidation by cytochrome bd studied with ubiquinone-2 analogs. *J. Biochem.* **2006**, *139*, 779−788.
(75) Biagini, G. A.; Fisher, N.; Shone, A. E.; Mubaraki, M. A.; Srivastava, A.; Hill, A.; Antoine, T.; Warman, A. J.; Davies, J.; Pidathala, C.; Amewu, R. K.; Leung, S. C.; Sharma, R.; Gibbons, P.; Hong, D. W.; Pacorel, B.; Lawrenson, A. S.; Charoensutthivarakul, S.; Taylor, L.; Berger, O.; Mbekeani, A.; Stocks, P. A.; Nixon, G. L.; Chadwick, J.; Hemingway, J.; Delves, M. J.; Sinden, R. E.; Zeeman, A. M.; Kocken, C. H.; Berry, N. G.; O'Neill, P. M.; Ward, S. A. Generation of quinolone antimalarials targeting the *Plasmodium falciparum* mitochondrial respiratory chain for the treatment and prophylaxis of malaria. *Proc. Natl. Acad. Sci. U.S.A.* **2012**, *109*, 8298−8303.
(76) Sviriaeva, E.; Subramanian Manimekalai, M. S.; Gruber, G.; Pethe, K. Features and Functional Importance of Key Residues of the *Mycobacterium tuberculosis* Cytochrome bd Oxidase. *ACS Infect. Dis.* **2020**, *6*, 1697−1707.
(77) Lee, B. S.; Hards, K.; Engelhart, C. A.; Hasenoehrl, E. J.; Kalia, N. P.; Mackenzie, J. S.; Sviriaeva, E.; Chong, S. M. S.; Manimekalai, M. S. S.; Koh, V. H.; Chan, J.; Xu, J.; Alonso, S.; Miller, M. J.; Steyn, A. J. C.; Gruber, G.; Schnappinger, D.; Berney, M.; Cook, G. M.; Moraski, G. C.; Pethe, K. Dual inhibition of the terminal oxidases eradicates antibiotic-tolerant *Mycobacterium tuberculosis*. *EMBO Mol. Med.* **2021**, *13*, No. e13207.

https://doi.org/10.1021/acsinfecdis.2c00283
ACS Infect. Dis. XXXX, XXX, XXX−XXX

(78) Meunier, B.; Madgwick, S. A.; Reil, E.; Oettmeier, W.; Rich, P. R. New Inhibitors of the Quinol Oxidation Sites of Bacterial Cytochromes Bo and Bd. *Biochemistry* **1995**, *34*, 1076−1083.
(79) Lu, P.; Asseri, A. H.; Kremer, M.; Maaskant, J.; Ummels, R.; Lill, H.; Bald, D. The anti-mycobacterial activity of the cytochrome bcc inhibitor Q203 can be enhanced by small-molecule inhibition of cytochrome bd. *Sci. Rep.* **2018**, *8*, No. 2625.
(80) Lu, P.; Heineke, M. H.; Koul, A.; Andries, K.; Cook, G. M.; Lill, H.; van Spanning, R.; Bald, D. The cytochrome bd-type quinol oxidase is important for survival of *Mycobacterium smegmatis* under peroxide and antibiotic-induced stress. *Sci. Rep.* **2015**, *5*, No. 10333.
(81) Höfle, G.; Bohlendorf, B.; Fecker, T.; Sasse, F.; Kunze, B. Semisynthesis and Antiplasmodial Activity of the Quinoline Alkaloid Aurachin E. *J. Nat. Prod.* **2008**, *71*, 1967−1969.
(82) Li, X. W.; Herrmann, J.; Zang, Y.; Grellier, P.; Prado, S.; Muller, R.; Nay, B. Synthesis and biological activities of the respiratory chain inhibitor aurachin D and new ring versus chain analogues. *Beilstein J. Org. Chem.* **2013**, *9*, 1551−1558.
(83) Harikishore, A.; Chong, S. S. M.; Ragunathan, P.; Bates, R. W.; Gruber, G. Targeting the menaquinol binding loop of mycobacterial cytochrome bd oxidase. *Mol. Diversity* **2021**, *25*, 517−524.
(84) Hopfner, S. M.; Lee, B. S.; Kalia, N. P.; Miller, M. J.; Pethe, K.; Moraski, G. C. Structure guided generation of thieno[3,2-d]-pyrimidin-4-amine *Mycobacterium tuberculosis* bd oxidase inhibitors. *RSC Med. Chem.* **2021**, *12*, 73−77.
(85) Biagini, G. A.; Fisher, N.; Shone, A. E.; Mubaraki, M. A.; Srivastava, A.; Hill, A.; Antoine, T.; Warman, A. J.; Davies, J.; Pidathala, C.; Amewu, R. K.; Leung, S. C.; Sharma, R.; Gibbons, P.; Hong, D. W.; Pacorel, B.; Lawrenson, A. S.; Charoensutthivarakul, S.; Taylor, L.; Berger, O.; Mbekeani, A.; Stocks, P. A.; Nixon, G. L.; Chadwick, J.; Hemingway, J.; Delves, M. J.; Sinden, R. E.; Zeeman, A. M.; Kocken, C. H.; Berry, N. G.; O'Neill, P. M.; Ward, S. A. Generation of quinolone antimalarials targeting the *Plasmodium falciparum* mitochondrial respiratory chain for the treatment and prophylaxis of malaria. *Proc. Natl. Acad. Sci. U.S.A.* **2012**, *109*, 8298−8303.
(86) Ehrt, S.; Schnappinger, D.; Rhee, K. Y. Metabolic principles of persistence and pathogenicity in *Mycobacterium tuberculosis*. *Nat. Rev. Microbiol.* **2018**, *16*, 496−507.
(87) Abrahams, K. A.; Cox, J. A.; Spivey, V. L.; Loman, N. J.; Pallen, M. J.; Constantinidou, C.; Fernandez, R.; Alemparte, C.; Remuinan, M. J.; Barros, D.; Ballell, L.; Besra, G. S. Identification of novel imidazo[1,2-a]pyridine inhibitors targeting M. tuberculosis QcrB. *PLoS One* **2012**, *7*, No. e52951.
(88) Pethe, K.; Bifani, P.; Jang, J.; Kang, S.; Park, S.; Ahn, S.; Jiricek, J.; Jung, J.; Jeon, H. K.; Cechetto, J.; Christophe, T.; Lee, H.; Kempf, M.; Jackson, M.; Lenaerts, A. J.; Pham, H.; Jones, V.; Seo, M. J.; Kim, Y. M.; Seo, M.; Seo, J. J.; Park, D.; Ko, Y.; Choi, I.; Kim, R.; Kim, S. Y.; Lim, S.; Yim, S. A.; Nam, J.; Kang, H.; Kwon, H.; Oh, C. T.; Cho, Y.; Jang, Y.; Kim, J.; Chua, A.; Tan, B. H.; Nanjundappa, M. B.; Rao, S. P.; Barnes, W. S.; Wintjens, R.; Walker, J. R.; Alonso, S.; Lee, S.; Kim, J.; Oh, S.; Oh, T.; Nehrbass, U.; Han, S. J.; No, Z.; Lee, J.; Brodin, P.; Cho, S. N.; Nam, K.; Kim, J. Discovery of Q203, a potent clinical candidate for the treatment of tuberculosis. *Nat. Med.* **2013**, *19*, 1157−1160.
(89) Koul, A.; Vranckx, L.; Dhar, N.; Gohlmann, H. W.; Ozdemir, E.; Neefs, J. M.; Schulz, M.; Lu, P.; Mortz, E.; McKinney, J. D.; Andries, K.; Bald, D. Delayed bactericidal response of *Mycobacterium tuberculosis* to bedaquiline involves remodelling of bacterial metabolism. *Nat. Commun.* **2014**, *5*, No. 3369.
(90) van Heeswijk, R. P. G.; Dannemann, B.; Hoetelmans, R. M. Bedaquiline: a review of human pharmacokinetics and drug-drug interactions. *J. Antimicrob. Chemother.* **2014**, *69*, 2310−2318.
(91) Pontali, E.; Sotgiu, G.; Tiberi, S.; D'Ambrosio, L.; Centis, R.; Migliori, G. B. Cardiac safety of bedaquiline: a systematic and critical analysis of the evidence. *Eur. Respir. J.* **2017**, *50*, No. 1701462.
(92) Nixon, G. L.; Moss, D. M.; Shone, A. E.; Lalloo, D. G.; Fisher, N.; O'Neill, P. M.; Ward, S. A.; Biagini, G. A. Antimalarial pharmacology and therapeutics of atovaquone. *J. Antimicrob. Chemother.* **2013**, *68*, 977−985.
(93) Nixon, G. L.; Pidathala, C.; Shone, A. E.; Antoine, T.; Fisher, N.; O'Neill, P. M.; Ward, S. A.; Biagini, G. A. Targeting the mitochondrial electron transport chain of *Plasmodium falciparum*: new strategies towards the development of improved antimalarials for the elimination era. *Future Med. Chem.* **2013**, *5*, 1573−1591.
(94) Barton, V.; Fisher, N.; Biagini, G. A.; Ward, S. A.; O'Neill, P. M. Inhibiting Plasmodium cytochrome bc1: a complex issue. *Curr. Opin. Chem. Biol.* **2010**, *14*, 440−446.
(95) Miroux, B.; Walker, J. E. Over-production of proteins in *Escherichia coli*: Mutant hosts that allow synthesis of some membrane proteins and globular proteins at high levels. *J. Mol. Biol.* **1996**, *260*, 289−298.
(96) Fisher, N.; Warman, A. J.; Ward, S. A.; Biagini, G. A. Chapter 17 Type II NADH: quinone oxidoreductases of *Plasmodium falciparum* and *Mycobacterium tuberculosis* kinetic and high-throughput assays. *Methods Enzymol.* **2009**, *456*, 303−320.
(97) Karakashev, D.; Galabova, D.; Simeonov, I. A simple and rapid test for differentiation of aerobic from anaerobic bacteria. *World J. Microbiol. Biotechnol.* **2003**, *19*, 233−238.
(98) Fisher, N.; Majid, R. A.; Antoine, T.; Al-Helal, M.; Warman, A. J.; Johnson, D. J.; Lawrenson, A. S.; Ranson, H.; O'Neill, P. M.; Ward, S. A.; Biagini, G. A. Cytochrome *b* mutation Y268S conferring atovaquone resistance phenotype in malaria parasite results in reduced parasite bc_1 catalytic turnover and protein expression. *J. Biol. Chem.* **2012**, *287*, 9731−9741.
(99) Jones, G.; Willett, P.; Glen, R. C.; Leach, A. R.; Taylor, R. Development and validation of a genetic algorithm for flexible docking. *J. Mol. Biol.* **1997**, *267*, 727−748.
(100) Kuhn, B.; Fuchs, J. E.; Reutlinger, M.; Stahl, M.; Taylor, N. R. Rationalizing Tight Ligand Binding through Cooperative Interaction Networks. *J. Chem. Inf. Model.* **2011**, *51*, 3180−3198.
(101) Hartkoorn, R. C.; Chandler, B.; Owen, A.; Ward, S. A.; Squire, S. B.; Back, D. J.; Khoo, S. H. Differential drug susceptibility of intracellular and extracellular tuberculosis, and the impact of P-glycoprotein. *Tuberculosis* **2007**, *87*, 248−255.
(102) Biagini, G. A.; Fisher, N.; Berry, N.; Stocks, P. A.; Meunier, B.; Williams, D. P.; Bonar-Law, R.; Bray, P. G.; Owen, A.; O'Neill, P. M.; Ward, S. A. Acridinediones: selective and potent inhibitors of the malaria parasite mitochondrial bc1 complex. *Mol. Pharmacol.* **2008**, *73*, 1347−1355.
(103) Kuboyama, M.; Yong, F. C.; King, T. E. Studies on cytochrome oxidase. *J. Biol. Chem.* **1972**, *247*, 6375−6383.

https://doi.org/10.1021/acsinfecdis.2c00283
ACS Infect. Dis. XXXX, XXX, XXX−XXX